AMERICAN SOCIETY FOR MICROBIOLOGY | mBio®

RESEARCH ARTICLE
Molecular Biology and Physiology

Identification of Fis1 Interactors in *Toxoplasma gondii* Reveals a Novel Protein Required for Peripheral Distribution of the Mitochondrion

Kylie Jacobs,[a] Robert Charvat,[b] Gustavo Arrizabalaga[a,c]

[a]Department of Microbiology and Immunology, Indiana University School of Medicine, Indianapolis, Indiana, USA
[b]Department of Biology, University of Findlay, Findlay, Ohio, USA
[c]Department of Pharmacology and Toxicology, Indiana University School of Medicine, Indianapolis, Indiana, USA

ABSTRACT *Toxoplasma gondii*'s single mitochondrion is very dynamic and undergoes morphological changes throughout the parasite's life cycle. During parasite division, the mitochondrion elongates, enters the daughter cells just prior to cytokinesis, and undergoes fission. Extensive morphological changes also occur as the parasite transitions from the intracellular environment to the extracellular environment. We show that treatment with the ionophore monensin causes reversible constriction of the mitochondrial outer membrane and that this effect depends on the function of the fission-related protein Fis1. We also observed that mislocalization of the endogenous Fis1 causes a dominant-negative effect that affects the morphology of the mitochondrion. As this suggests that Fis1 interacts with proteins critical for maintenance of mitochondrial structure, we performed various protein interaction trap screens. In this manner, we identified a novel outer mitochondrial membrane protein, LMF1, which is essential for positioning of the mitochondrion in intracellular parasites. Normally, while inside a host cell, the parasite mitochondrion is maintained in a lasso shape that stretches around the parasite periphery where it has regions of coupling with the parasite pellicle, suggesting the presence of membrane contact sites. In intracellular parasites lacking LMF1, the mitochondrion is retracted away from the pellicle and instead is collapsed, as normally seen only in extracellular parasites. We show that this phenotype is associated with defects in parasite fitness and mitochondrial segregation. Thus, LMF1 is necessary for mitochondrial association with the parasite pellicle during intracellular growth, and proper mitochondrial morphology is a prerequisite for mitochondrial division.

IMPORTANCE *Toxoplasma gondii* is an opportunistic pathogen that can cause devastating tissue damage in the immunocompromised and congenitally infected. Current therapies are not effective against all life stages of the parasite, and many cause toxic effects. The single mitochondrion of this parasite is a validated drug target, and it changes its shape throughout its life cycle. When the parasite is inside a cell, the mitochondrion adopts a lasso shape that lies in close proximity to the pellicle. The functional significance of this morphology is not understood and the proteins involved are currently not known. We have identified a protein that is required for proper mitochondrial positioning at the periphery and that likely plays a role in tethering this organelle. Loss of this protein results in dramatic changes to the mitochondrial morphology and significant parasite division and propagation defects. Our results give important insight into the molecular mechanisms regulating mitochondrial morphology.

KEYWORDS Fis1, *Toxoplasma*, membrane contact site, mitochondrion

Citation Jacobs K, Charvat R, Arrizabalaga G. 2020. Identification of Fis1 interactors in *Toxoplasma gondii* reveals a novel protein required for peripheral distribution of the mitochondrion. mBio 11:e02732-19. https://doi.org/10.1128/mBio.02732-19.

Editor Jon P. Boyle, University of Pittsburgh

Address correspondence to Gustavo Arrizabalaga, garrizab@iu.edu.

Received 12 October 2019
Accepted 23 December 2019
Published 11 February 2020

Toxoplasma gondii is an opportunistic protozoan parasite that can infect nearly any nucleated cell in a wide range of warm-blooded organisms. This promiscuity contributes to *T. gondii* being one of the most widespread and successful parasites in the world. It has been estimated that approximately one-third of the world's human population is infected with *Toxoplasma* (1). While infections in otherwise healthy adults are asymptomatic, in immunocompromised individuals and lymphoma patients, infections can lead to toxoplasmic encephalitis, among other complications. Additionally, in congenital infections, toxoplasmosis can lead to blindness, severe neurological problems, or even death given the immature nature of the fetal immune system. One interesting feature of *Toxoplasma* is its single mitochondrion, which is very large and extends to the periphery of the cell. In addition to its plant-like features, such as tubular cristae, the *Toxoplasma* mitochondrion has a streamlined mitochondrial genome consisting of three genes, *cox1*, *cob*, and *cox3*, encoding three proteins (2). These unique features of the mitochondrion, along with its essentiality for parasite survival, make it an interesting drug target. The clinical effectiveness of the mitochondrial inhibitor atovaquone against *Toxoplasma* and related parasites highlights the validity of this organelle as a target for antiparasitic therapy (3). Aspects of the apicomplexan mitochondrion that remain unexplored as a potential target are its morphology and division. Thus, in-depth understanding of the regulation of mitochondrial morphology and dynamics in *Toxoplasma* could reveal novel therapeutic targets.

The mitochondrion of *Toxoplasma* is highly dynamic and exhibits significant morphological changes during the parasite's life cycle and in response to various stressors. As there is only one mitochondrion per parasite, its division is tightly coordinated with the division of the rest of the parasite (4). *Toxoplasma* divides by endodyogeny, a specialized process through which two daughter cells form within the mother parasite and during which each organelle is either made *de novo* or elongated and divided for incorporation into the daughter parasites. The mitochondrion divides very late in this process and is not incorporated into the daughter parasites until the parasites have almost completely emerged from the mother parasite (4). Typically, the mitochondrial division machinery is made up of three components: a fission protein to recruit proteins necessary for division, adaptor proteins to provide a scaffold, and a dynamin-related protein to cause the final scission of the mitochondrion (5). *Toxoplasma* does not appear to carry any genes that encode homologs to the adaptor proteins or any of the additional recruiting proteins found in mammals, such as Mff or Mid49/51 (6). It does contain genes that encode one homolog of the fission protein Fis1 (TGGT1_263323) and three potential dynamin-related proteins (Drps): DrpA, DrpB, and DrpC. *T. gondii* DrpA (TgDrpA) and TgDrpB have been shown to be required for apicoplast replication and secretory organelle biogenesis, respectively (7, 8). TgDrpC is divergent from the typical Drp due to the absence of a conserved GTPase effector domain, which is generally required for function. We recently showed that TgDrpC localizes to cytoplasmic puncta that redistribute to the growing edge of the daughter parasites during endodyogeny and that it interacts with proteins that exhibit homology to those involved in vesicle transport (9, 10).

After repeated division cycles, the parasites egress from the cell and are exposed to the extracellular environment, where the mitochondrion alters its morphology. When *Toxoplasma* is within a host cell, it maintains its mitochondrion in a lasso shape that spans the parasite's periphery and is adjacent to the parasite pellicle (2, 4, 11). Immediately after egress, the mitochondrion retracts from the periphery of the parasite and transitions to a "sperm-like" morphology, where the majority of mitochondrial material is at the apical end of the parasite with a tail of material extending toward the basal end (11). Prolonged exposure to the extracellular environment results in transition to a completely collapsed mitochondrion. Upon reinvasion, the mitochondrion returns to the "lasso" shape almost immediately (11). Electron microscopy of parasites with lasso-shaped mitochondrion reveals the presence of regions of close abutment between the outer mitochondrion membrane (OMM) and the inner membrane complex (IMC), in which the membranes retain a constant distance over stretches of 100 nm to

1,000 nm (11). The average distance between the OMM and IMC was calculated to be approximately 25 nm, which would suggest the presence of membrane contact sites (11, 12). Neither the functional significance nor the components of the proposed contact between the mitochondrion and the pellicle are known.

We have also observed that the mitochondrion of *Toxoplasma* significantly changes its morphology in response to exposure to the anticoccidial drug monensin. Monensin is a sodium hydrogen exchanger that induces oxidative stress (13) and autophagic cell death (14). We demonstrate that monensin's effect on mitochondrion morphology is reversible, suggesting that *Toxoplasma* has mechanisms to rearrange the mitochondrial structure in response to drug-induced stress. As the mitochondrion appears broken down upon monensin treatment, we investigated the role of the fission machinery on this phenomenon. Here, we show that monensin induces a reversible constriction of the outer mitochondrial membrane and that this effect is in part dependent on the fission protein Fis1. We also show that, although Fis1 is not required for parasite survival, mislocalization of Fis1 away from the outer mitochondrial membrane results in aberrant mitochondrial morphology. We hypothesize that the dominant-negative effect caused by mislocalization of Fis1 is due to misdirecting critical proteins away from the mitochondrion. Accordingly, we identified interactors of Fis1. One such interactor, TGGT1_265180, proved to be required for parasite growth, division, and mitochondrial segregation. Importantly, the mitochondria of intracellular parasites lacking this Fis1 interactor are not lasso shaped but instead are collapsed away from the parasite periphery. Accordingly, we hypothesize that this novel protein is part of the proposed scaffold that mediates membrane contact sites between the mitochondrion and parasite pellicle.

RESULTS

Monensin-induced mitochondrial remodeling is reversible. We had previously observed that treatment with the polyether ionophore monensin induced gross morphological changes in *Toxoplasma*, including alterations in the Golgi apparatus and mitochondrion (13). In particular, the mitochondrion, which under normal growth conditions appears as a lasso along the periphery of the parasite, becomes fragmented in appearance upon monensin treatment (Fig. 1A). To assess whether this effect on the parasite mitochondrion was reversible, parasites were treated with either vehicle or 1 mM monensin for 12 h, followed by a 12-h recovery period on normal growth medium. Under vehicle-treated conditions, parasites exhibited intact mitochondria in greater than 91% of vacuoles (Fig. 1A and B). In contrast, after 12 h of monensin treatment, only 6.25% $\pm$ 11.8% of vacuoles contained parasites with intact mitochondria, congruent with previous findings (Fig. 1A and B). Interestingly, this phenotype is reversed when the drug is removed, and parasites are allowed to recover for 12 h. After the 12-h recovery period, in 79.5% $\pm$ 5.5% of vacuoles, all parasites show normal mitochondrial morphology (Fig. 1A and B). Of note, there was no observed reduction in the total number of parasite-containing vacuoles in the cultures in which the drug was removed and in culture in which the drug was not removed, indicating a genuine recovery and not an expansion of surviving parasites.

To determine whether mitochondrial remodeling is a generalized drug response, parasites were challenged with atovaquone and myxothiazol, both cytochrome bc_1 complex inhibitors, and pyrimethamine, a dihydrofolate reductase inhibitor not known to affect mitochondrial function. After 12 h of atovaquone treatment, only 27.3% $\pm$ 15.5% of parasites showed intact mitochondria, and as observed with monensin, this effect was reversed by the removal of drug and a 12-h drug-free recovery period (75.8% $\pm$ 13.0% intact mitochondria [Fig. 1C]). In contrast, a lethal dose of myxothiazol (50 ng/ml [15, 16]) had little effect on mitochondrial morphology, with 82% $\pm$ 5.4% of vacuoles with intact mitochondrion after treatment, which increased to 91.5% $\pm$ 5.2% upon drug removal, although these effects did not meet statistical significance (Fig. 1C). Upon pyrimethamine treatment, 60.3% $\pm$ 17.0% of parasites had aberrant mitochondrial morphology. As this level did not change with statistical

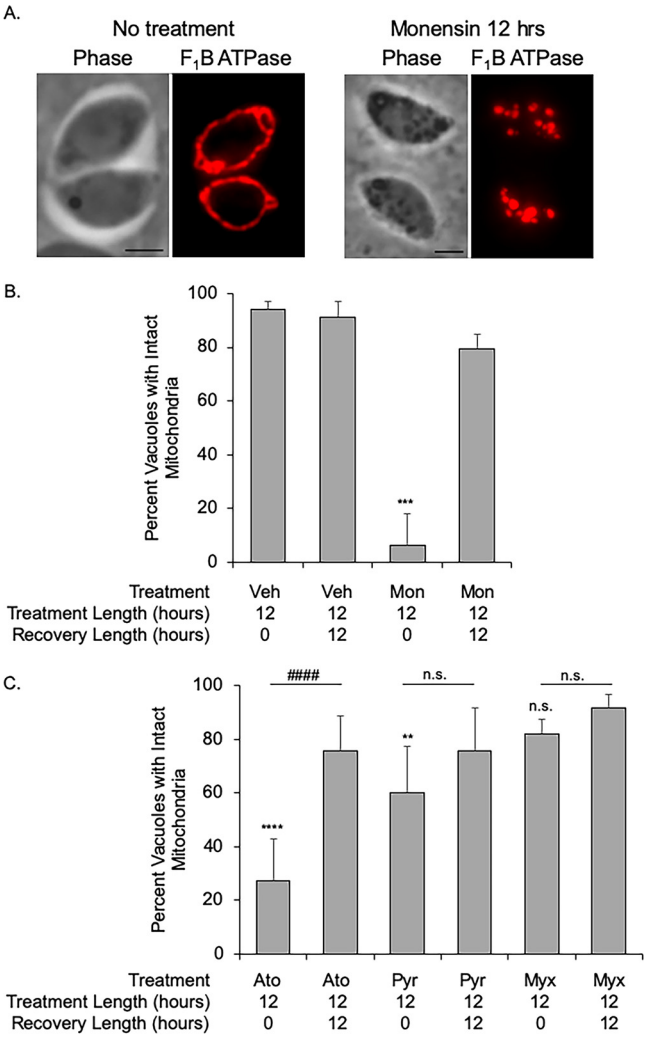

FIG 1 Drug-induced mitochondrial disruption is reversible. To determine the effects of drugs on mitochondrial morphology, intracellular parasites were treated with various agents. Parasite mitochondrial morphology was examined by visualizing the inner mitochondrial membrane (IMM)-localized F_1B ATPase through immunofluorescence microscopy. (A) Left panels show mitochondrion after treatment with vehicle, while right panels show effect of treatment with 1 mM monensin for 12 h. The mitochondria in the vehicle-treated parasites shown are considered intact, while in the drug-treated parasites shown, they are considered disrupted. Bars, 2 μm. (B) The percentage of vacuoles with intact mitochondria is presented for parasites that were treated with vehicle (Veh) or with monensin (Mon) for 12 h or treated with monensin, followed by a 12-h recovery period. (C) The effects of the antiparasitic drug atovaquone (Ato) (100 nM), pyrimethamine (Pyr) (100 μM), and myxothiazol (Myx) (50 ng/ml) on the mitochondrion were assessed. With each drug we also tested the effect of a 12-h recovery period after 12 h of drug treatment. For all graphs, 100 vacuoles for each condition were enumerated at random, and the data are presented as the averages $\pm$ standard deviations (SD) (error bars) from three independent experiments. One-way ANOVA with a *posthoc* Tukey test was utilized for statistical analysis. In panel B, ***, $P < 0.0001$ in comparison to other treatments. In panel C, each drug treatment was compared to vehicle treatment (****, $P < 0.0001$; **, $P < 0.007$; n.s., not significant), and each treatment was compared to treatment followed by recovery (####, $P < 0.001$).

significance upon removal of drug (75.5% $\pm$ 16.2%), the disruption of the mitochondrion observed is likely the consequence of parasite death and not the temporary and reversible rearrangement seen with monensin and atovaquone. Taken together, reversible mitochondrial disruption does not appear to be a generalized mechanism for responding to stress induced via drug challenge. Moreover, *Toxoplasma* possesses the capacity for reversible mitochondrial rearrangement in response to specific drug-induced stress.

A fission protein homolog localizes to the outer mitochondrial membrane. The most striking aspect of monensin treatment in *Toxoplasma* is the disruption of mito-

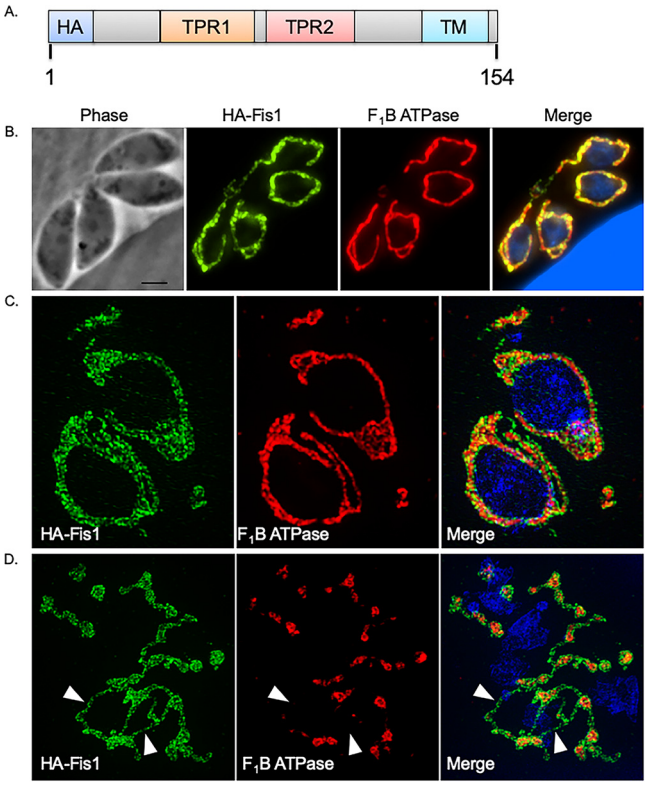

FIG 2 Fis1 localizes to the *Toxoplasma* outer mitochondrial membrane, which remains intact after monensin treatment. To determine the subcellular distribution of the fission protein homolog Fis1, a parasite strain expressing an ectopic copy of Fis1 including an N-terminal HA epitope tag was generated. (A) Illustration shows the exogenously expressed epitope-tagged Fis1. Protein domains in Fis1 are indicated: tetratricopeptide repeat domains TPR1 and TPR2 and transmembrane (TM) domain. (B to D) Intracellular parasites of the (HA)Fis1-expressing strain were analyzed by IFA using antibodies against the HA tag to detect Fis1 (in green) and against the *Toxoplasma* F_1B ATPase protein to delineate the inner mitochondrial membrane (in red) using either a Nikon Eclipse 80i microscope (B) or an OMX 3D-SIM superresolution imaging system (C and D). (D) Intracellular parasites were treated for 8 h with monensin (1 ng/ml). White arrowheads in panel D demarcate regions of Fis1 staining without the ATPase signal. Bar, 2 μm.

chondrial morphology, producing what appears to be a fragmented organelle. A survey of the *Toxoplasma* database (ToxoDB) to identify homologs involved in mitochondrial dynamics revealed that the genome of *Toxoplasma* is rather bereft of proteins that participate in the fusion and fission processes. However, we were able to identify a protein (TGGT1_263323) with homology to the fission 1 (Fis1) protein from higher eukaryotes. TGGT1_263323, referred to hereafter as Fis1, is a 154-amino-acid protein and contains two tetratricopeptide (TPR) domains, a C-terminal transmembrane (TM) domain, followed by a 3-amino-acid C-terminal sequence (CTS). In previous work focused on the characterization of membrane anchor domains in *Toxoplasma*, we showed through transient transfection of an N-terminal hemagglutinin (HA)-tagged Fis1 that it localized to the mitochondrion (17). In order to further characterize the localization and function of Fis1, we established a parasite strain stably expressing an N-terminally HA epitope-tagged version of Fis1 under the control of the SAG1 promoter (Fig. 2A). Immunofluorescence assay (IFA) of intracellular parasites of this strain (RHΔ*hpt*+HAFis1) confirmed that Fis1 localized to the parasite mitochondrion by colocalization with F_1B ATPase protein, which is located in the inner mitochondrial membrane (IMM) (Fig. 2B). Superresolution imaging shows that the Fis1 signal envelops the signal from F_1B ATPase (Fig. 2C). This strongly suggests that, as expected for Fis1 proteins, Fis1 localizes to the outer mitochondrial membrane.

Since we had observed mitochondrial fragmentation following monensin treatment, we next sought to examine whether drug challenge resulted in altered localization of

Fis1. RHΔ*hpt*+HAFis1 parasites were treated for 8 h with monensin and prepared for superresolution imaging. As anticipated, we observed fragmented mitochondrial morphology when examining the localization of F_1B ATPase (Fig. 2D). Some of the mitochondrial fragments were encircled by the Fis1 protein, as one would expect for a protein in the outer mitochondrion membrane (OMM) (Fig. 2D). Importantly, we also identified mitochondrial fragments that appeared to be connected by filaments of Fis1 (white arrowheads [Fig. 2D]). These superresolution images revealed that the OMM remains intact following the 8-h monensin treatment despite the punctate appearance of the IMM. Thus, the observed effect of monensin treatment on mitochondrial morphology is not a true fragmentation but rather a constriction of the OMM in particular regions.

The Fis1 transmembrane domain is required for proper localization to the OMM. Our previous studies have shown that the TM domain of Fis1 is sufficient for mitochondrial targeting (17). To determine whether the TM is necessary for mitochondrial localization, we established a parasite strain expressing an exogenous copy of Fis1 with an N-terminal HA tag and truncated at the C terminus so as to lack the TM and CTS (Fig. 3A). Intracellular parasites of this strain were costained with antibodies against HA to detect Fis1ΔTM and against F_1B ATPase to visualize the mitochondrion (Fig. 3B). Fis1 lacking the TM appears to be distributed throughout the cytoplasm in a punctate pattern (Fig. 3B). A similar result was observed when the TM of the endogenous Fis1 was replaced by an HA epitope tag using homologous recombination (Fig. 3C). Eliminating the TM of the endogenous Fis1 shifted its localization from the mitochondrion to the cytoplasm (Fig. 3D). Thus, proper Fis1 localization to the OMM is dependent on its C-terminal transmembrane domain and CTS.

Mitochondrial morphology is altered by the mislocalization of Fis1. When analyzing the localization of the truncated endogenous Fis1, we noted that the morphology of the mitochondrion appeared abnormal. Instead of the typical lasso seen in wild-type parasites (Fig. 1 and 2), the mitochondrion in parasites of the RHΔ*ku80*:Fis1ΔTM strain appeared to contain additional branches as well as unconnected strands, a phenotype that seemed to increase as the parasites underwent several rounds of division (Fig. 3D). In the RHΔ*ku80*:Fis1ΔTM strain, 60.4% ± 7.5% of vacuoles had parasites with atypical mitochondria (i.e., extraneous branches and strands). This is in contrast to the parental strain in which only 12.7% ± 3.4% of vacuoles had parasites with atypical mitochondria (Fig. 3E). These observations suggest that mislocalizing the endogenous Fis1 alters the typical mitochondrial morphology.

RHΔ*ku80*:Fis1ΔTM parasites are less susceptible to monensin-induced mitochondrial disruption. The Fis1 protein in higher eukaryotes is responsible for fission of stressed and damaged mitochondria in order to maintain a healthy organelle pool. Thus, we next sought to determine the effect of Fis1 mislocalization in parasites undergoing monensin drug challenge. Parasites were treated with vehicle or monensin for 12 h. Cultures were fixed and examined by immunofluorescence microscopy, and vacuoles with fragmented F_1B ATPase signal were tallied. In the absence of treatment, the percentage of parasites with punctate F_1B ATPase staining was statistically similar for the parental and mutant strains (18.6% ± 12.4% versus 23.8% ± 17.2). Following monensin treatment of parental parasites, an increase from 18.6% ± 14.8% to 67.6% ± 10.5% punctate mitochondria was observed for the parental strain (Fig. 4A). In RHΔ*ku80*:Fis1ΔTM parasites, an increase from 23.8% ± 17.2% to 51.0% ± 9.3% punctate mitochondria was recorded after drug challenge (Fig. 4A). The percent increase between the vehicle- and monensin-treated parasites was determined, and the increase in punctate mitochondria was statistically greater for the parental parasites than for the RHΔ*ku80*:Fis1ΔTM parasites, 49.0% ± 6.1% versus 27.2% ± 9.6, respectively (Fig. 4B).

The phenotypes observed with the RHΔ*ku80*:Fis1ΔTM parasites could be due to either the absence of Fis1 at the mitochondrion or a dominant-negative effect from the mislocalized truncated protein. To differentiate between these possibilities, we next sought to determine how genetic ablation of Fis1 would affect the parasite's ability

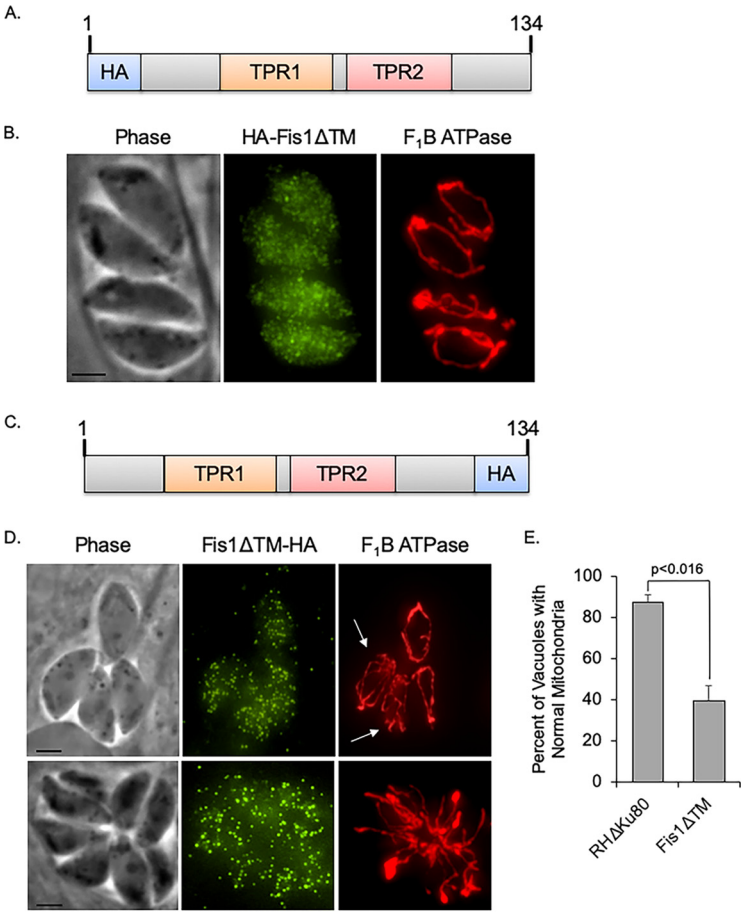

FIG 3 Fis1 localization is dependent on its transmembrane domain. To determine the necessity of the TM domain for localization of Fis1, we engineered strains in which either an exogenous or the endogenous Fis1 lacked the transmembrane domain. (A) Schematic of the exogenous HA-FisΔTM. (B) Parasites expressing HA-FisΔTM were costained for the exogenous Fis1 (in green) and the mitochondrial F_1B ATPase (in red). Bar, 2 μm. (C) Schematic of endogenous Fis1 in which TM has been replaced by an HA epitope (Fis1ΔTM-HA). (D) Intracellular parasites of the strain expressing the truncated Fis1 were stained with antibodies against the HA tag (green) to detect Fis1ΔTM and antibodies against F_1B ATPase (red) to detect mitochondria. White arrows indicate abnormal appearing mitochondria. Bars, 2 μm. (E) The frequency of Fis1ΔTM-HA-expressing parasites with abnormal mitochondrial morphology (extraneous fragments or branches) was examined and compared to that of the parental Δ*ku80* strain. In three independent experiments, parasite vacuoles from 15 random fields of view were enumerated, and the data are presented as percentage of vacuoles with normal mitochondrial morphology ± SD. Student's *t* test was employed for determining statistical significance.

to respond to monensin challenge and undergo mitochondrial remodeling. Employing the CRISPR/Cas9 system, RHΔ*hpt*+HAFis1 parasites ectopically expressing the N-terminally HA epitope-tagged Fis1 were either transfected with a single guide RNA (sgRNA) that would target both the endogenous and exogenous Fis1 gene or a sgRNA for the nonessential uracil phosphoribosyltransferase (UPRT) gene as a control. Parasites were immediately used to infect human foreskin fibroblasts (HFFs) on coverslips and grown in culture for 16 h. Infected cultures were then treated with vehicle or monensin for 12 h. After treatment, parasites were fixed and IFA was performed with staining for HA to detect Fis1 and F_1B ATPase to visualize the mitochondria (see Fig. S1 in the supplemental material). We then compared the mitochondrial morphology in Fis1 sgRNA-transfected parasites lacking HA signal to that of control sgRNA-transfected parasites with HA signal. To control for the effects of Cas9, which is fused to green fluorescent protein (GFP) (18), we analyzed the mitochondrial morphology only in parasites with nuclear GFP signal. In vehicle-treated parasites, there was no significant difference between parasites lacking HA-tagged Fis1 expression and parasites trans-

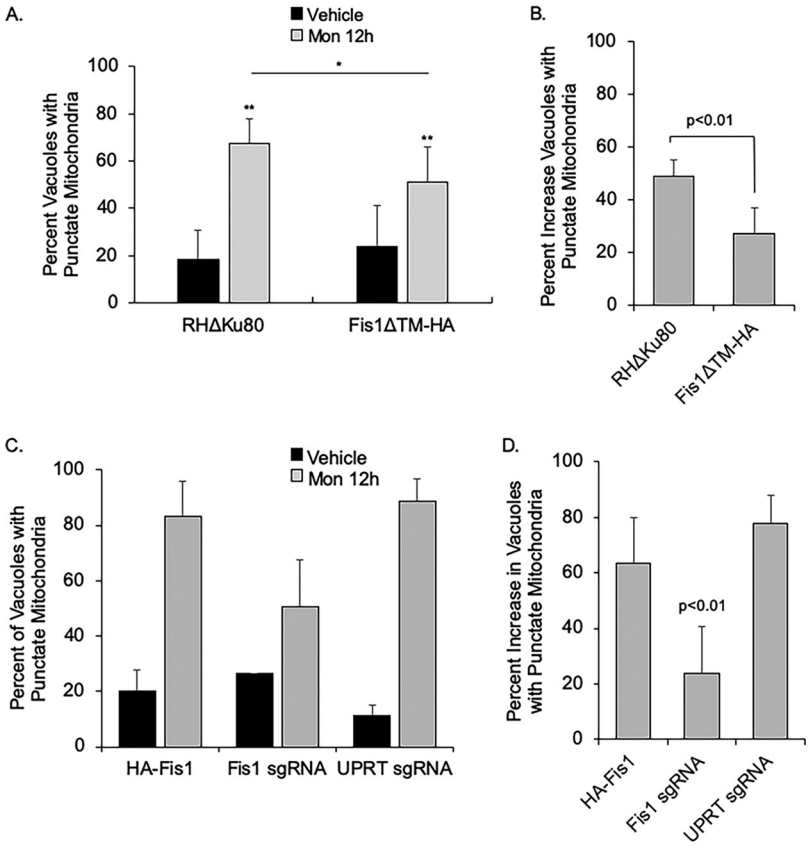

FIG 4 Disrupting Fis1 reduces monensin-induced mitochondrial remodeling. The ability of monensin to induce mitochondrial remodeling was assessed in strains expressing a mislocalized Fis1 or lacking Fis1. (A) Parasites in which the endogenous Fis1 lacks the TM domain were treated with vehicle or monensin for 12 h. Parasite vacuoles were enumerated from 10 random fields of view for each strain and condition. The data are the averages from four independent experiments and are presented as percentage of vacuoles with punctate morphology ± SD. Statistical analysis was provided by one-way ANOVA *posthoc* Tukey test, (**, $P < 0.001$ compared to vehicle; *, $P < 0.01$). (B) Data from panel A were analyzed to compare the number of vacuoles with punctate mitochondrion in untreated and treated parasites for each strain. Data are displayed as percent increase of vacuoles with punctate mitochondria upon treatment ± SD. (C) RHΔ*hpt* parasites ectopically expressing the N-terminally HA-tagged Fis1 were transfected with a plasmid expressing Cas9 and either a Fis1-specific sgRNA or the nonspecific UPRT sgRNA. After transfection, parasites were immediately infected into HFFs on coverslips. Following approximately 16 h in culture, cultures were treated with vehicle or monensin for 12 h, and an IFA to monitor mitochondrial morphology was performed. The data presented are the averages for six coverslips from two independent transfections. Bars represent percent punctate mitochondria ± SD. Statistical significance was determined via two-way ANOVA, treatment $P < 0.0.0001$, genotype $P = 0.006$, genotype X treatment $P = 0.0003$. (D) The percent increase in punctate mitochondria between treatment and no treatment for the data shown in panel C was calculated and presented as averages ± SD.

fected with UPRT sgRNA compared to the control parasites still expressing Fis1 (Fig. 4C and Fig. S1). Interestingly, in contrast to what we observed with mislocalized Fis1, complete lack of Fis1 did not affect the mitochondrial morphology. Thus, it appears that Fis1 lacking the TM domain imparts a dominant-negative effect on mitochondrial morphology.

As expected, monensin treatment of the Cas9/sgRNA-transfected parasites resulted in an increase in the number of vacuoles containing punctate F_1B ATPase signal. Control nontransfected parasites and those transfected with the UPRT sgRNA possessed 83.3% ± 12.8% and 88.8% ± 7.7% punctate mitochondria, respectively (Fig. 4C). However, parasites lacking the HA-tagged Fis1 signal displayed significantly fewer vacuoles with disrupted mitochondria upon monensin treatment, comprising only 50.5% ± 16.9% of the vacuoles (Fig. 4C). The percent increase in the number of vacuoles with punctate mitochondria for the parasites deficient in HA-tagged Fis1

TABLE 1 Proteins identified as Fis1 interactors through a yeast two-hybrid screen[a]

Gene ID	Product description	PrBS[b]
TGGT1_215520	**Hypothetical protein**	**A**
TGGT1_218560	**Acetyl-CoA carboxylase ACC2**	**B**
TGGT1_222800	Glycogen synthase, putative	B
TGGT1_265180	**Hypothetical protein**	**B**
TGGT1_224270	Hypothetical protein	C
TGGT1_293840	Hypothetical protein	C
TGGT1_201390	Hypothetical protein	D
TGGT1_226050	Hypothetical protein	D
TGGT1_237015	GRA43	D
TGGT1_246720	**Hypothetical protein**	**D**
TGGT1_247700	AP2 domain transcription factor AP2XII-4	D
TGGT1_284620	Hypothetical protein	D
TGGT1_286470	AGC kinase	D
TGGT1_287980	FHA domain-containing protein	D
TGGT1_297770	Hypothetical protein	D
TGGT1_299670	Hypothetical protein	D
TGGT1_304990	**Guanylate-binding protein**	**D**
TGGT1_321370	**Hypothetical protein**	**D**
TGGT1_321450	**Myb family DNA-binding domain-containing protein**	**D**

[a]Proteins that were also identified in the mitochondrial proteome (35) are shown in boldface type. ID, identifier; acetyl-CoA, acetyl coenzyme A.
[b]Predicted biological scores (PrBS) are confidence scores, with A indicating the highest confidence of interaction and D the lowest confidence of interaction (19, 20).

expression was significantly lower than for either control parasite populations, 23.9% ± 17% versus 63.3% ± 16.8% and 77.8% ± 10.2%, respectively (Fig. 4D). Two-way analysis of variance (ANOVA) analysis indicated that there was both a treatment and genotype effect and that the effects interact. Overall, these data indicate that complete lack of Fis1 does not affect mitochondrial morphology in untreated parasites but significantly decreases monensin-induced mitochondrial remodeling, indicating that Fis1 is partially required for constriction of the IMM in response to treatment with the ionophore.

A putative Fis1 interactor localizes to the OMM. Mislocalization of the endogenous Fis1 results in a dominant-negative phenotype in terms of mitochondrial morphology. We hypothesize that this is the result of mislocalization of Fis1 interactors required at the mitochondrion for normal morphology. To identify these potential interactors, we employed a yeast two-hybrid (Y2H) interaction screen. Using full-length Fis1 as bait, 46 million clones were screened for Y2H interaction and 247 were selected for identification. The putative interactors were then given a confidence score based on the likelihood of interaction with Fis1 (19, 20). This resulted in 24 potential interactors with a global predicted biological score (PrBS) from A (highest confidence) to D (lowest confidence) (19, 20) (Table 1). To narrow down the list, we immunoprecipitated the exogenous HA-tagged Fis1 using HA-conjugated beads and analyzed the precipitated complex by mass spectroscopy. For a control, we used the parental RHΔ*hpt* strain, which does not express the hemagglutinin tag. Through this analysis, we identified 11 putative interactors that had at least five peptides in the Fis1 sample and no peptides in the control sample (see Table S1 in supplemental material). Among these interactors, only one was also identified in the Y2H interaction screen, TGGT1_265180.

To determine the localization of TGGT1_265180, we introduced a C-terminal myc epitope tag to the endogenous gene. IFA assays of the resulting strain show that, like Fis1, TGGT1_265180 is localized to the mitochondrion of intracellular parasites (Fig. 5A). This association with the mitochondrion persists during parasite division (Fig. 5B). To determine whether the protein is associated with the outside or inside of the mitochondrion, we performed IFA after permeabilization with various concentrations of digitonin using detection of F_1B ATPase to monitor mitochondrial permeabilization (Fig. 5C). When using 0.01% digitonin, we can detect both F_1B ATPase and

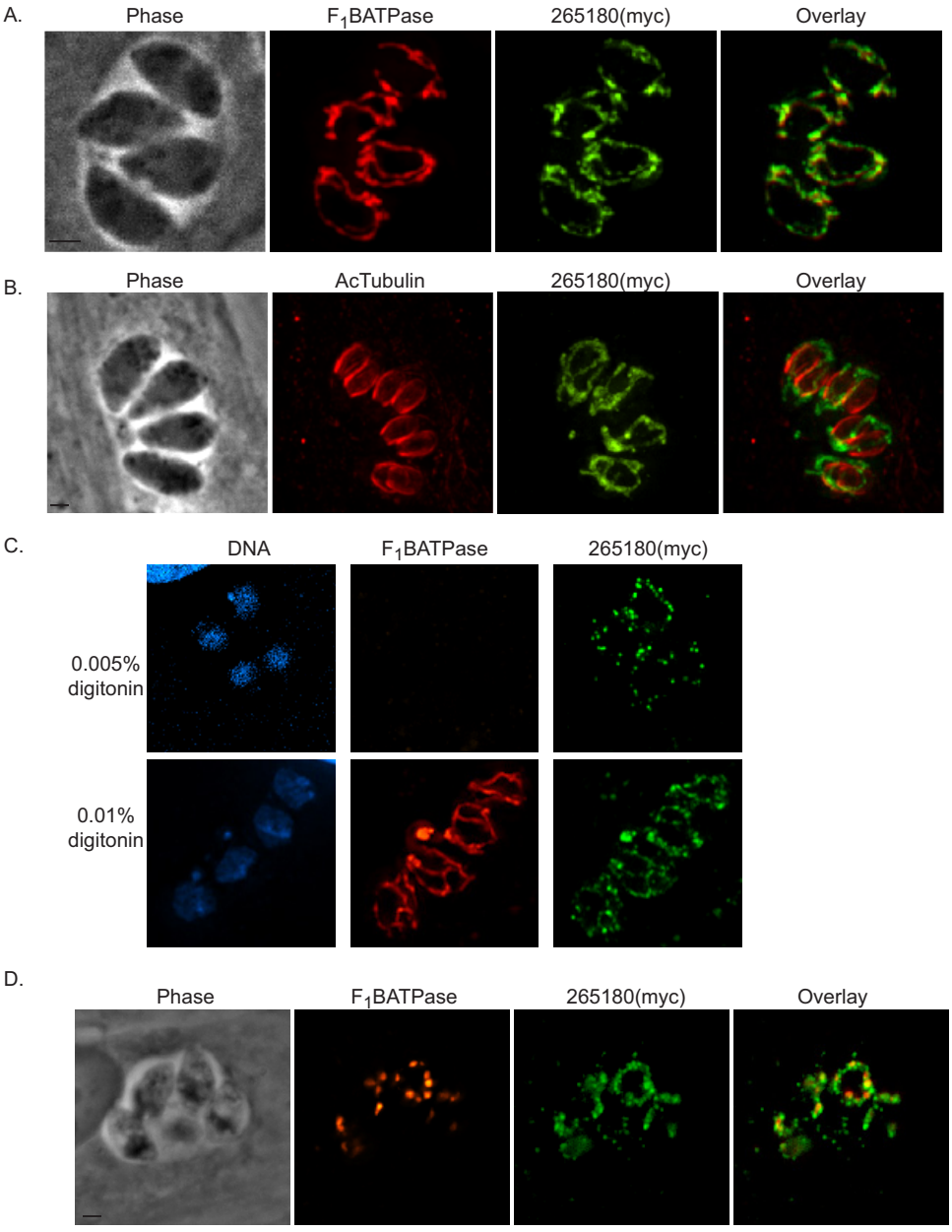

FIG 5 Fis1 interactor TGGT1_265180 localizes to the outer mitochondrial membrane. To investigate the localization of TGGT1_265180, we introduced sequences encoding an N-terminal myc tag to the endogenous locus. (A) Intracellular parasites of the TGGT1_265180(myc)-expressing strain were stained for mitochondrial F_1B ATPase (red) and myc (green). (B) Intracellular parasites of the same strain were stained for myc (green) and acetylated tubulin (red), which clearly demarcates daughter parasites during division. (C) Intracellular parasites of the TGGT1_265180(myc)-expressing strain were fixed and permeabilized with either 0.005% or 0.01% digitonin before staining for the IMM protein F_1B ATPase (red) and myc (green). TGGT1_265180 can be detected when F_1B ATPase remains inaccessible to the antibodies, suggesting that it is associated with the OMM. (D) TGGT1_265180(myc) parasites were treated with 5 mM monensin for 5 h. Mitochondrial morphology was monitored by IFA for TGGT1_265180(myc) (green) and F_1B ATPase (red). Bars, 2 μm.

TGGT1_265180 (Fig. 5C). In contrast, using 0.005% digitonin allows for detection of TGGT1_265180 but not F_1B ATPase. This result mimics what is seen with Fis1 (Fig. S2), and thus, like Fis1, TGGT1_265180 likely associates with the OMM and faces the cytoplasm of the parasite (Fig. 5C). Association with the OMM was confirmed by treatment with monensin. After treating TGGT1_265180(myc) expressing parasites with monensin, we observed a pattern similar to that of Fis1 in which fragments containing the IMM marker F_1B ATPase are surrounded and connected by TGGT1_265180 (Fig. 5D).

Thus, TGGT1_265180 localizes to the OMM, as expected for a bona fide interactor of Fis1.

Localization of TGGT1_265180 is partially dependent on proper Fis1 localization. Despite its association with the OMM, TGGT1_265180 has no predicted transmembrane domains or posttranslational modifications that would suggest membrane interaction. Therefore, we hypothesize that the localization of TGGT1_265180 occurs via protein-protein interaction. To test this idea, we transfected parasites with an ectopic copy of either full-length or truncated TGGT1_265180 carrying a C-terminal HA epitope tag and under the control of the TGGT1_265180 promoter (Fig. 6A). The truncated form lacks the C-terminal 92 amino acids, which represent the region of the protein that was identified through the Y2H screen as interacting with Fis1, referred to as the selected interaction domain (SID). As expected, the full-length ectopic copy localized to the mitochondrion (Fig. 6A). However, deletion of the SID resulted in the mislocalization of the protein to the cytoplasm (Fig. 6A). These data indicate that the C-terminal SID is necessary for proper mitochondrial localization.

To investigate whether localization of TGGT1_265180 to the mitochondrion is through an interaction with Fis1, we added a myc epitope tag to the endogenous TGGT1_265180 in the strain in which Fis1 lacks its TM (RHΔ*ku80*:Fis1ΔTM) and is mislocalized to the cytoplasm. In this strain, TGGT1_265180 does not colocalize with the mislocalized Fis1 but appears to accumulate toward the basal end of the parasites in a pattern that does not resemble normal mitochondrial localization (Fig. 6B). To further analyze the localization of TGGT1_265180 in the RHΔ*ku80*:Fis1ΔTM parasite line, we costained for F_1B ATPase (Fig. 6C). While we observed some overlap between the TGGT1_265180 and F_1B ATPase signals, TGGT1_265180 was also detected away from the mitochondrion (Fig. 6C). Interestingly, we observed that the TGGT1_265180(myc) signal, as detected through IFA, appeared to be much weaker in the Fis1ΔTM strain than in the parental strain (Fig. 6C). To quantitate this observation, we performed Western blotting from both strains probing for TGGT1_265180(myc) (Fig. 6D). This analysis corroborated that indeed the levels of endogenous TGGT1_265180 are significantly reduced when Fis1 is mislocalized away from the mitochondrion (Fig. 6D). We quantitated the levels of TGGT1_265180 in both strains by performing densitometry of three independent Western blots using the surface antigen SAG1 as a loading control and determined that the level of TGGT1_265180 in the RHΔ*ku80*:Fis1ΔTM is 23.2% $\pm$ 8.7% of that in the parental strain. In conjunction, these results indicate that TGGT1_265180 associates with the mitochondrion via its C terminus and that its localization and stability are at least in part dependent on Fis1.

265180 knockout affects parasite fitness in tissue culture. Based on a genome-wide CRISPR screen, TGGT1_265180 was assigned a relative fitness phenotype score of -1.65, which indicates that, while its absence would negatively affect parasite fitness, it is likely not essential, making its genetic disruption possible (21). Accordingly, we employed double homologous recombination to replace the coding sequence of TGGT1_265180 with a drug selection marker (Fig. 7A). Proper integration of the knockout construct in stably transfected clones was confirmed by PCR (Fig. 7B). To test the effect of the knockout on parasite propagation, we used a standard growth assay in which the same number of parasites (parental or mutant parasites) were allowed to infect human fibroblasts and form plaques over a 5-day period. We observed a significant propagation defect in the Δ*265180* parasites, exhibited by both fewer and smaller plaques in comparison to the parental strain. To quantitate this defect, we counted the number of plaques formed by the parental and knockout strains in three separate experiments, each with experimental triplicates (Fig. 7C). The average number of plaques by the Δ*265180* was 30.2% $\pm$ 9.0% of that detected for the parental strain.

To confirm that the phenotype observed was due to the disruption of the target gene and not a secondary effect, we complemented the Δ*265180* strain with an exogenous copy of the TGGT1_265180 including a C-terminal HA epitope tag and

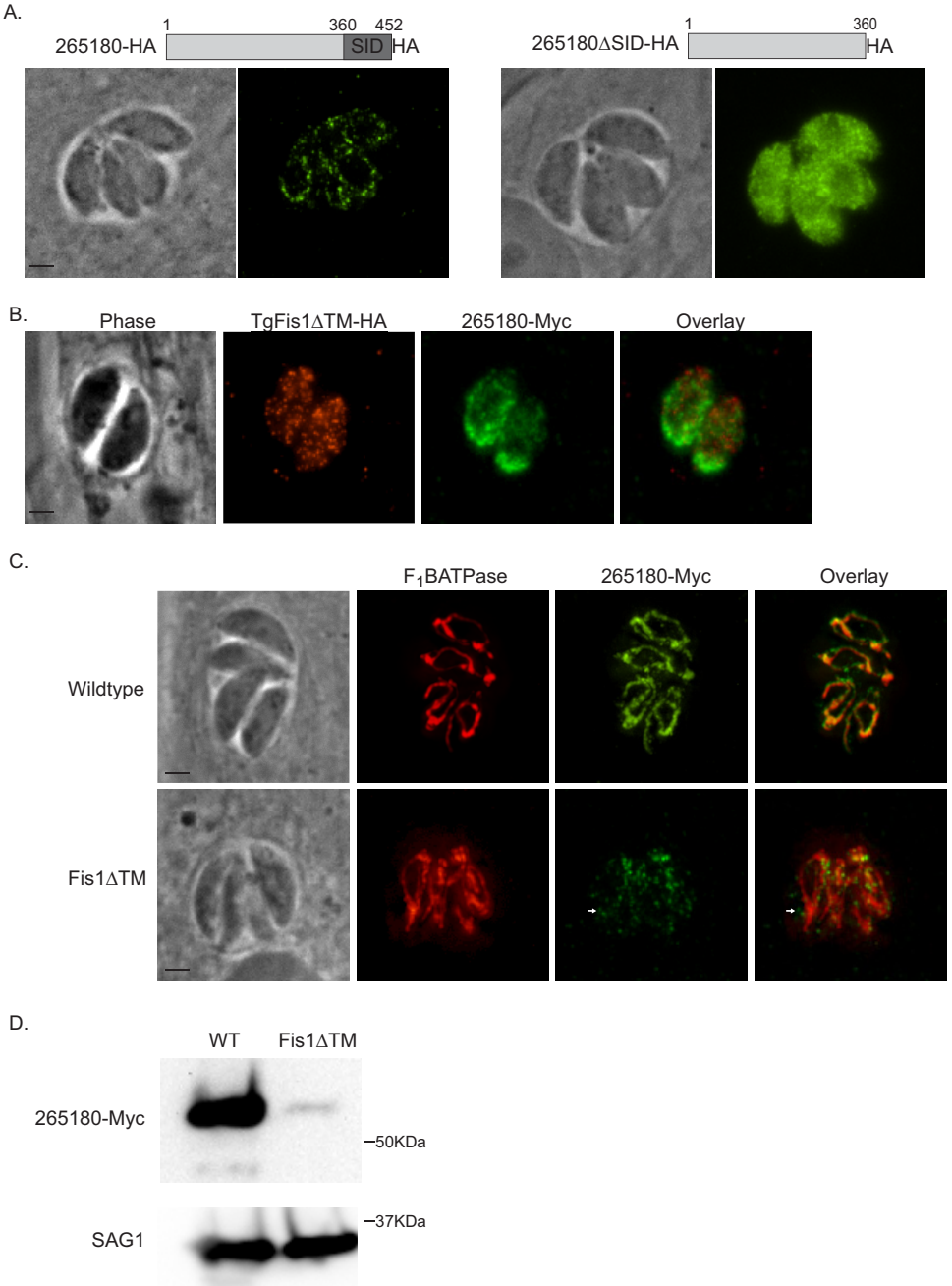

FIG 6 Association of TGGT1_265180 with the mitochondrion depends on Fis1. To investigate how TGGT1_265180 associates with the mitochondrion, we tested the roles of its C terminus and Fis1 on its localization. (A) Parasites were transfected with an exogenous copy of C-terminally HA-tagged wild-type TGGT1_265180 or with N-terminally HA-tagged TGGT1_265180 lacking the selected interaction domain (SID). The SID is the region of TGGT1_265180 that was identified as interacting with Fis1. Intracellular parasites expressing TGGT1_265180-HA (left) or TGGT1_265180ΔSID-HA (right) were stained for HA. (B) Intracellular FisΔTM-HA parasites expressing an endogenous copy of C-terminally myc-tagged TGGT1_265180 were probed for HA to detect Fis1 (red) and for myc to detect TGGT1_265180 (green). (C) Wild-type or FisΔTM-HA parasites endogenously expressing TGGT1_265180-Myc were stained for F_1B ATPase (red) and myc (green) to monitor localization of TGGT1_265180. Bars, 2 μm. (D) Representative Western blot of extract from wild-type (WT) and Fis1ΔTM parasites expressing TGGT1_265180-myc probed for myc (top blot) and SAG1 (bottom blot) as a loading control.

driven by its own promoter. As the knockout strain lacks Ku80 and does not effectively allow for random integration, the exogenous copy was directed to the remnants of the Ku80 locus using CRISPR/Cas9. In addition to complementing with the wild-type TGGT1_265180, we transfected the knockout strain with the truncated version

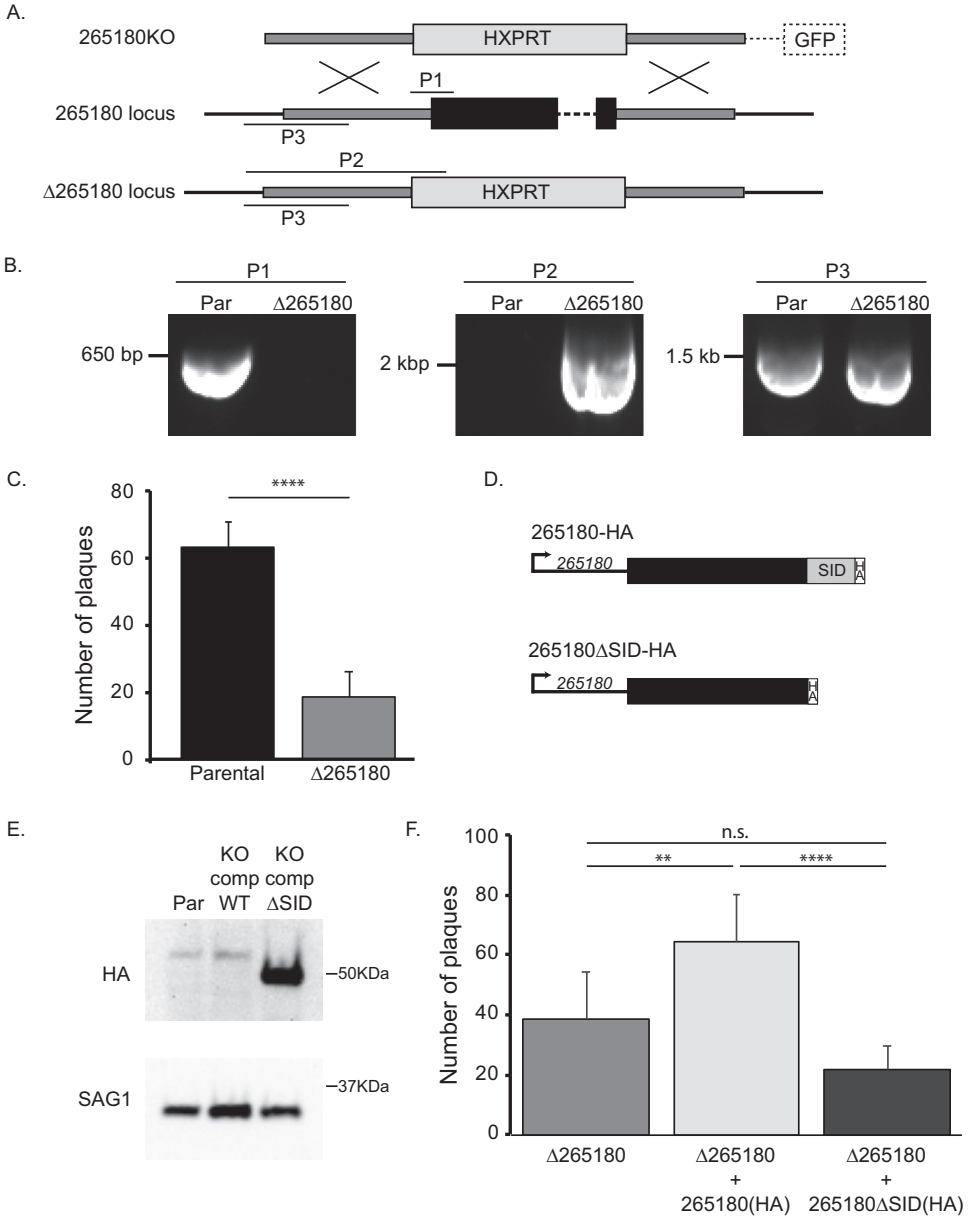

FIG 7 Knockout of TGGT1_265180 affects parasite propagation. To investigate the role of TGGT1_265180 in parasite fitness, we established knockout and complemented strains. (A) Schematic of strategy implemented to disrupt the TGGT1_265180 by replacing the coding sequences by the selectable marker *HXPRT*. On top is the vector used to drive the gene replacement, which includes *HXPRT* flanked by areas of homology to the TGGT1_265180 locus (dark gray boxes) and a downstream copy of GFP that is not integrated upon the desired double homologous recombination and can be used as a negative selectable marker. Endogenous TGGT1_265180 is depicted in the middle with coding sequences represented by a black box. The bottom drawing shows the expected result from gene replacement in the knockout strain. P1, P2, and P3 indicate the PCR amplicons that were used to confirm integration. P1 would be detected only from parental parasites, P2 only from knockout parasites, and P3 from both. (B) PCR products from reactions to detect P1, P2, and P3 in the parental strain and the established Δ*265180* clone. (C) Average number of plaques per well for either parental or knockout strains after 4-day incubation period. Plaque assays were done in biological and technical triplicates, with error bars representing SD. Statistical analysis was performed by the *t* test (****, $P < 0.0001$). (D) Diagrams depict the two constructs used for complementation: TGGT1_265180-HA and TGGT1_265180ΔSID-HA. SID is the selected interaction domain identified through the two-hybrid screen. (E) Representative Western blot of a strain in which the endogenous TGGT1_265180 includes a HA epitope tag (parental [Par]), and the knockout strain complemented with wild-type TGGT1_265180-HA (KO comp WT) or with TGGT1_265180ΔSID-HA (KO comp ΔSID) probed for HA (top blot) and for SAG1 (bottom blot) as a loading control. (F) Average number of plaques per well for each strain after 4-day incubation period. Plaque assays were done in biological and technical triplicates, with error bars representing SD. Statistical analysis was performed by one-way ANOVA (****, $P < 0.0001$; **, $P < 0.0019$; n.s., not significant).

TGGT1_265180ΔSID, which does not localize to the mitochondrion (Fig. 7D). Western blots showed that both complemented strains expressed proteins of the expected size (Fig. 7E). Interestingly, while the wild-type complement expression level is similar to that of the endogenous levels, the truncated copy appears to be expressed at a much higher level (Fig. 7E). Plaque assays of both the Δ*265180* + 265180(HA) and Δ*265180* + 265180ΔSID(HA) strains were performed in parallel with the knockout strain (Fig. 7F). The average number of plaques by the Δ*265180* + 265180(HA) was 64.5% ± 15.8, which is significantly higher than both the knockout and truncated complemented strains (Fig. 7F). Δ*265180* + 265180ΔSID(HA) had a lower average number of plaques (21.6% ± 8.0) than that of the knockout (38.8% ± 15.3), but this difference was not statistically significant. These results indicate that proper localization of TGGT1_265180 is necessary to rescue the growth phenotype seen in tissue culture.

265180 disrupts the normal morphology of the mitochondrion. As TGGT1_265180 is associated with the mitochondrion, we assessed mitochondrial morphology in the knockout parasites. In intracellular parasites, the mitochondrion maintains what is referred to as a lasso shape that abuts the periphery of the parasite (11) (Fig. 2 and 8A). However, based on staining with antibodies against F_1B ATPase, the mitochondrion of Δ*265180* parasites exhibit an altered mitochondrial morphology, with the bulk of the mitochondrial material concentrated at one end of the parasite (Fig. 8A). In contrast, disruption of TGGT1_265180 did not affect the morphology of the apicoplast, rhoptries, or endoplasmic reticulum (Fig. S3). Introduction of the wild-type TGGT1_265180 to the knockout strain complements the mitochondrial phenotype (Fig. 8B). In contrast, the truncated TGGT1_265180ΔSID, which is not localized to the mitochondrion, does not rescue the collapsed mitochondrion phenotype (Fig. 8C). The phenotype of the knockout and complemented strains was quantitated by determining the percentage of parasites with normal and abnormal mitochondrion morphology. Normally, the *Toxoplasma* mitochondrion retracts from the periphery of the parasite during egress and changes its morphology to what has been described as sperm-like and collapsed (11). Interestingly, we observed all three morphologies normally associated with extracellular parasites (lasso, sperm-like, and collapsed) in intracellular parasites of the Δ*265180* strain (Fig. 9A). With the parental strain, the proportion of mitochondrial morphologies in intracellular parasites is 84.7% ± 2.1% lasso, 15.3% ± 2.1% sperm-like, and 0% collapsed. In contrast, for intracellular parasites of the Δ*265180* strain, the mitochondrial distribution is 6.0% ± 2.6% lasso, 50.0%% ± 2% sperm-like, and 44.0% ± 4.4% collapsed (Fig. 9B). As was the case for the plaquing phenotype, introduction of a wild-type copy of TGGT1_265180 partly rescues the morphological phenotype with 48.5% ± 4.4% of parasites exhibiting lasso-shaped mitochondrion, 49.2% ± 3.9% sperm-like, and only 2.3% ± 0.6% collapsed. Additionally, the truncated copy had a morphological distribution similar to that of the knockout strain (2.7% ± 2.3% lasso, 56.0% ± 10.1% sperm-like, and 41.4% ± 12.4% collapsed) and was significantly different from the distributions of the parental and complemented strains, which is consistent with defects seen in plaquing (Fig. 9B). Thus, TGGT1_265180 plays a crucial role in maintaining proper morphology of the mitochondrion. Consequently, we have dubbed this new protein lasso maintenance factor 1 (LMF1).

Disruption of LMF1 results in defects in mitochondrial segregation between daughter parasites. During our analysis of mitochondrial morphology in the LMF1 mutant strain, we noted various aberrant phenotypes that likely relate to parasite and mitochondrial division. *Toxoplasma* divides through a process called endodyogeny, where two daughter parasites form within a mother parasite (22). This results in a doubling in the number of parasites in a vacuole after each round of replication. We noted that vacuoles of the LMF1 strain often had abnormal numbers of parasites (i.e., not 2, 4, 8, etc.). We found that approximately 25.3% ± 5.1% of vacuoles in Δ*265180* parasites had odd numbers compared to 5.8% ± 2.9% in wild-type parasites and 13.7% ± 3.1% in the complemented strain

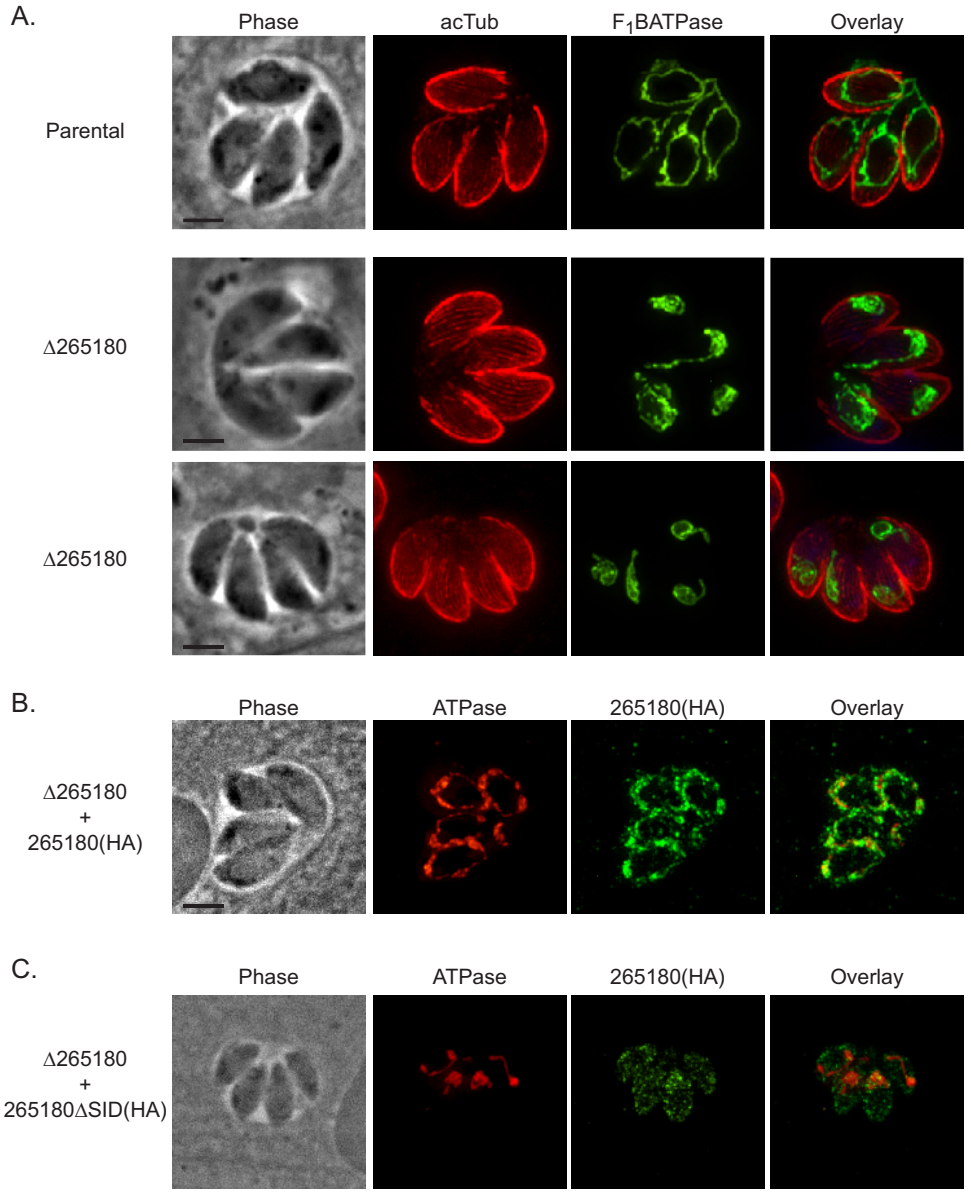

FIG 8 Mitochondrial morphology is disrupted by the absence of TGGT1_265180. To determine the effect of TGGT1_265180 ablation on the mitochondrion, knockout and complemented parasites were analyzed by IFA. (A) Intracellular parasites of the parental or Δ*265180* strain were stained for F_1B ATPase (green) to monitor mitochondrion and for acetylated tubulin (acTub) to detect the parasite cytoskeleton (red). (B and C) IFA of knockout parasites (Δ*265180*) transformed with either the wild-type [265180(HA)] or truncated [265180ΔSID(HA)] TGGT1_265180 with antibodies against F_1B ATPase (red) and HA (green). Bars, 2 μm.

(Fig. 10A). Interestingly, we also noticed numerous vacuoles in which some parasites lacked a mitochondrion based on the absence of F_1B ATPase staining (Fig. 10B, white arrows). When quantified, 16.2% $\pm$ 4.0% of vacuoles contained at least one parasite that did not have mitochondrial material compared to 0.3% $\pm$ 0.6% of RHΔ*ku80* parasites that were amitochondriate (Fig. 10B). As with the other phenotypes, exogenous expression of wild-type LMF1 complemented the phenotype with 6.0% $\pm$ 1.7% of vacuoles containing amitochondriate parasites. In addition to amitochondriate parasites, disruption of LMF1 also results in an accumulation of mitochondrial material outside parasites (Fig. 10C, white arrows). We determined that 30.9% $\pm$ 4.0% of vacuoles had extraparasitic mitochondrial material, which is three times greater than that of the parental parasite line (10.6% $\pm$ 3.2%). Interestingly, this particular

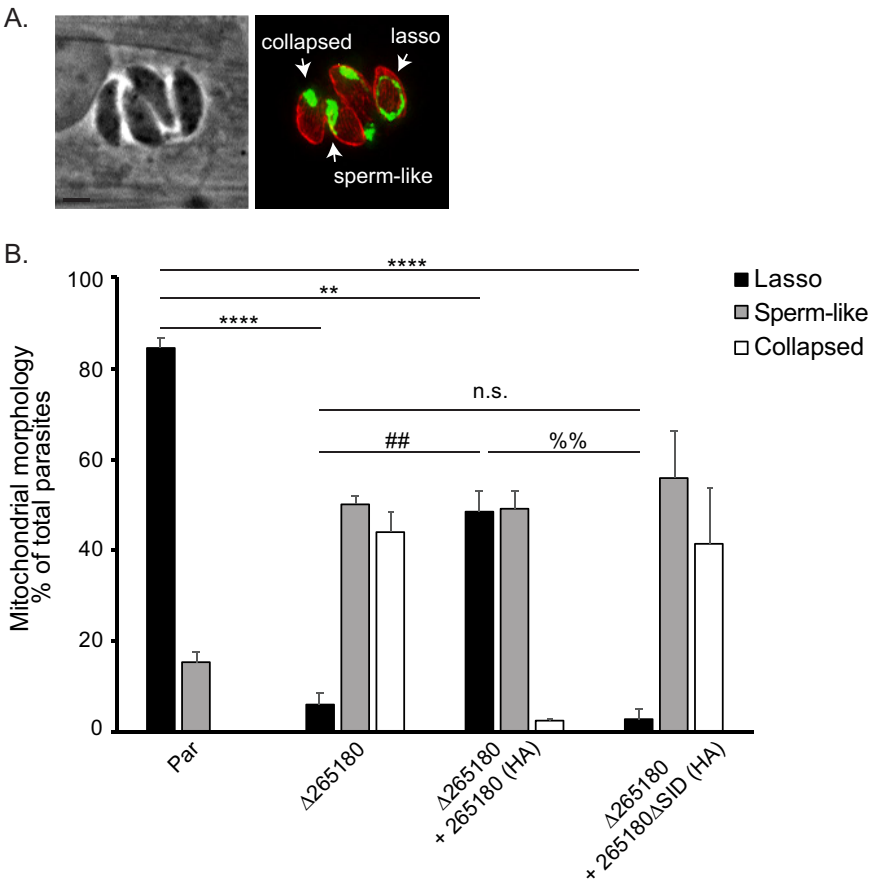

FIG 9 Intracellular parasites lacking TGGT1_265180 do not maintain their mitochondrion in the lasso conformation. To determine the penetrance of the mitochondrial phenotype observed in the Δ*265180* strain, the different morphological patterns observed were quantitated. (A) Intracellular parasites of the Δ*265180* strain stained for F_1B ATPase (green) and acetylated tubulin (red) exhibiting three distinct mitochondrial morphologies: lasso, collapsed, and sperm-like. Bar, 2 μm. (B) Percentage of parasites with each of the three different morphologies for the parental (par), knockout (Δ*265180*), and complemented [Δ*265180* + 265180(HA) and Δ*265180* + 265180ΔSID(HA)] strains. Data are average of biological triplicates, at least 50 vacuoles per sample were inspected. Error bars are SD. Statistics shown are ANOVA of percentage of parasites with lasso shape for each strain. ****, $P < 0.001$; **, $P < 0.004$; ##, $P < 0.003$; %%, $P < 0.002$; n.s., not significant.

phenotype was not complemented, as 28.3% ± 2.1% of Δ*265180* + 265180(HA) vacuoles contained extraparasitic material (Fig. 10C).

We hypothesize that these phenotypes (abnormal number of parasites, amitochondriate parasites, and extraparasitic mitochondria) are the result of aberrant segregation of the mitochondrion into the daughter cells during endodyogeny. Accordingly, we costained parental and knockout parasites for acetylated tubulin to detect daughter cells and for F_1B ATPase to monitor the mitochondrion (Fig. 11). During the early (E) stages of division, wild-type parasite mitochondria surround the forming daughter cells (Fig. 11A, top panels). As endodyogeny progresses to an intermediate (I) stage, the mitochondrion remains excluded from the daughters (Fig. 11A, middle panels). When the daughters have almost fully formed (late [L] stages), branches of mother mitochondria incorporate into the daughter parasites before emerging from the mother (Fig. 11A, bottom panels). When LMF1 is disrupted, the mitochondrion does not have the typical lasso shape and appears to associate with one of the two daughters instead of surrounding both (Fig. 11B, top panels [E]). As the daughters continue to form in the LMF1-deficient parasites, the mitochondrial material remains associated with one daughter or is completely excluded from the budding daughters (Fig. 11B, I panels). During the final stages of

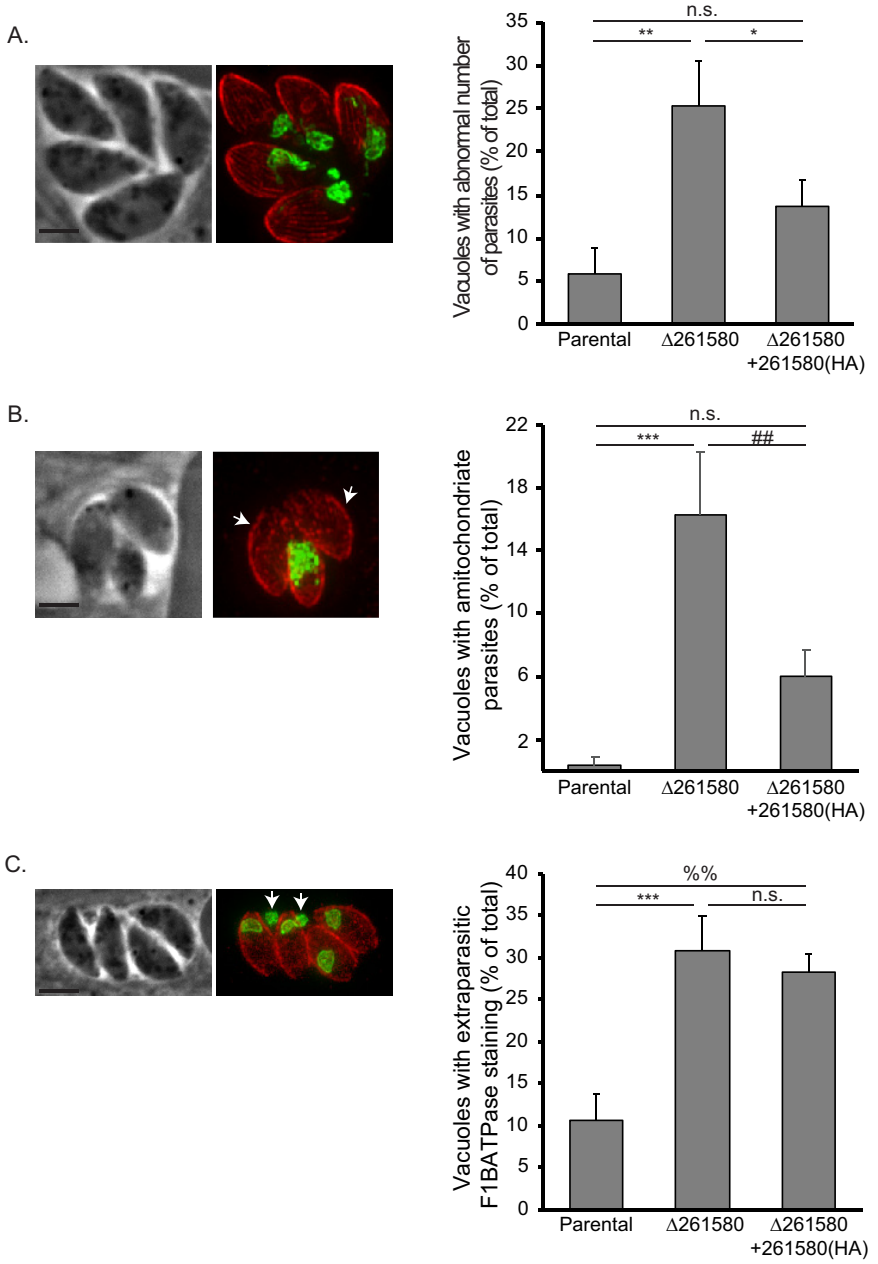

FIG 10 Parasites lacking TGGT1_265180 exhibit various division-related phenotypes. IFA of knockout parasites stained for F_1B ATPase (green) and acetylated tubulin (red) reveal various aberrant phenotypes. (A) The images on the left show a Δ*265180* vacuole containing five parasites rather than either four or eight as expected. The graph shows the percentage of vacuoles with abnormal number of parasites for the three strains. (B) Images show vacuole with amitochondriate parasites (arrows) based on the absence of F_1B ATPase signal. The graph shows the percentage of vacuoles with at least one amitochondriate parasite for each strain. (C) Images show a vacuole that contains parasites with F_1B ATPase signal outside the parasite and within the parasitophorous vacuole (arrows). Bars, 2 μm. The graph shows the percentage of vacuoles with this phenotype. For all graphs, $n = 3 \pm$ SD with at least 50 vacuoles per sample inspected. Statistical analysis was done with one-way ANOVA and a Tukey *posthoc* test. ***, $P < 0.0006$; **, $P < 002$; *, $P < 0.02$; ##, $P < 0.006$; %%, $P < 0.001$; n.s., not significant.

endodyogeny, some daughters seem to have received mitochondrial material, whereas others have not. This correlates to an accumulation of mitochondrial material outside the parasites (Fig. 11B, bottom three panels [L panels and unlabeled panels]). Therefore, disruption of LMF1 leads to defects in mitochondrial segregation during endodyogeny, which agrees with the aberrant phenotypes observed with mitochondrial shape and localization (Fig. 9 and 10).

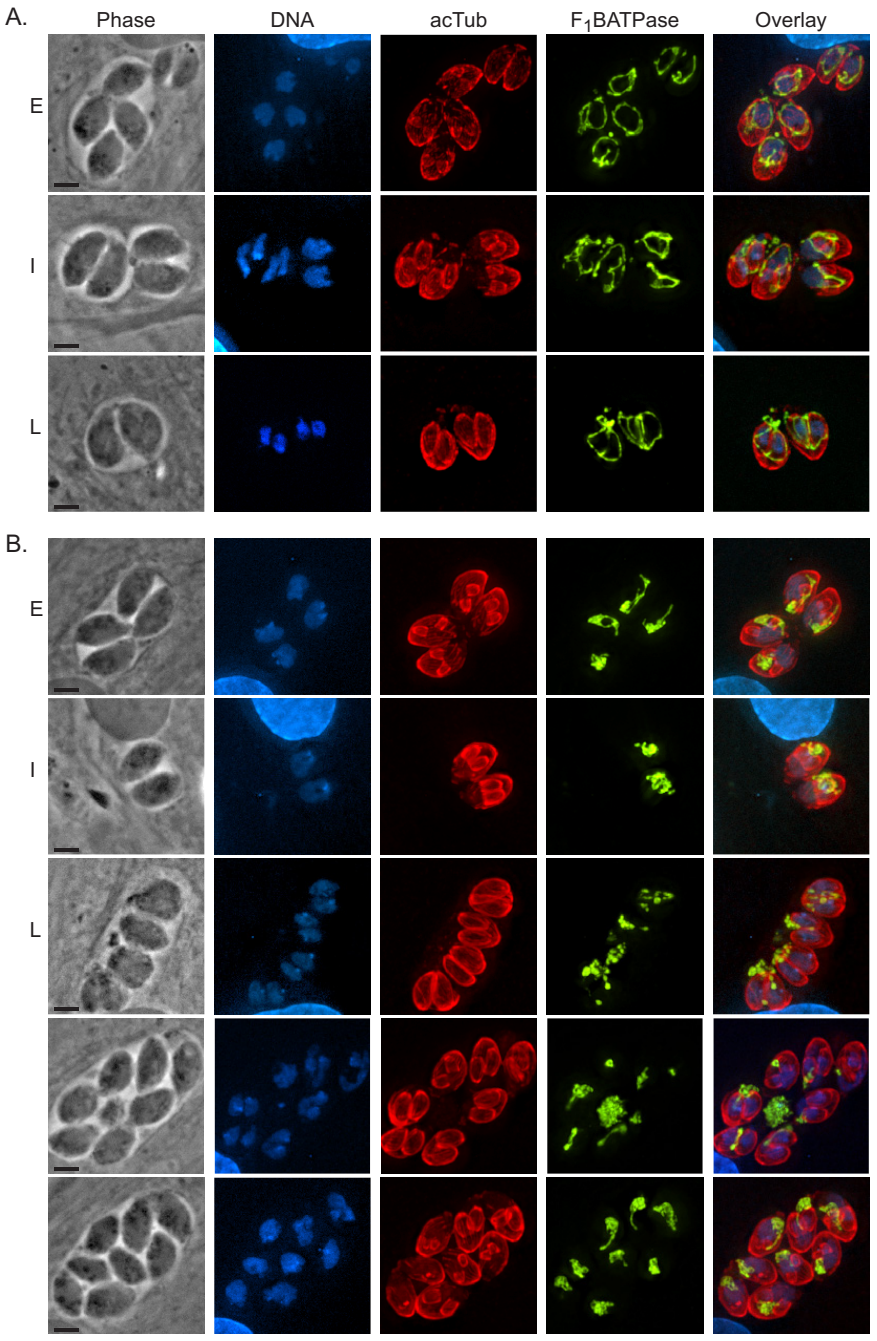

FIG 11 TGGT1_265180 disruption results in mitochondrial segregation defects. To examine mitochondrial dynamics during parasite division, IFAs of parasites during early (E), intermediate (I), and late (L) stages of endodyogeny were conducted. (A) IFAs of intracellular wild-type parasites. (B) IFAs of intracellular Δ*265180* (also known as LMF1) knockout parasites. In both panels A and B, the stage of division was determined by DAPI staining (blue) and acetylated tubulin (red), which demarcate budding daughters. Mitochondrial morphology was observed by staining with F_1B ATPase, shown here in green. Bars, 2 μm.

DISCUSSION

The single mitochondrion of the pathogen *Toxoplasma gondii* is highly dynamic, with its location and structure changing during various stages of the parasite's lytic cycle. As the last organelle to move from a live mother parasite into two nascent daughter cells, the morphology and position of the mitochondrion are tightly regulated during parasite division. Similarly, as the parasite moves from inside to outside host

cells, the mitochondrion morphology dramatically changes. While inside the host cell, *Toxoplasma*'s mitochondrion forms a lasso with multiple points of contact with the parasite pellicle and then quickly retracts from the parasite periphery to a collapsed bundle at the apical end as the parasites move to the extracellular space. In this study, we show that the mitochondrial morphology also changes under treatment with the antiparasitic drugs atovaquone and monensin. With drug treatment, the mitochondrion's outer membrane becomes constricted, causing the inner mitochondrial material to appear punctate. Importantly, this phenomenon is completely reversible, and upon removal of monensin, the mitochondrion returns to its typical shape. We also show that mitochondrial constriction upon monensin treatment is partly dependent on the presence of the fission protein Fis1 at the mitochondrion. Thus, we have discovered a mechanism by which the parasite reversibly restructures its mitochondrion.

The morphological changes experienced by the mitochondrion under monensin treatment are likely a response to stress and might represent a mechanism by which the parasite protects the mitochondrion from irreversible damage. Mitochondria from numerous organisms alter their morphology to respond to specific stressors, such as UV radiation and nutrient starvation (23–26). In conditions that damage mitochondrial DNA, such as cycloheximide and UV radiation, mitochondria hyperfuse (23). This phenomenon most likely occurs to complement damaged mitochondrial DNA and promote DNA mixing. Conditions that affect mitochondrial respiration, such as oligomycin and uncoupling agents, cause mitochondrial fragmentation (25, 26). Similarly, the mitochondria in *Saccharomyces cerevisiae* cultured in aerobic, respiratory conditions are more punctate, whereas when *S. cerevisiae* is cultured under anaerobic conditions, the mitochondria are branched and elongated (24). These data suggest that mitochondrial morphology is dependent upon environmental conditions and stressors. Therefore, the phenotype we see under monensin treatment is likely a protective mechanism for the mitochondrion against the effects of the ionophore.

As the effect of monensin is a reversible constriction along the outer mitochondrial membrane, we hypothesize that this phenomenon would require the mitochondrial fission machinery. The yeast mitochondrial fission machinery is the most well characterized, and it is comprised of the membrane-anchored protein Fis1p, which actively recruits other proteins to the mitochondria during fission like Mdv1 (mitochondrial division protein 1), which acts as an adaptor protein. Fis1p is then able to recruit a GTPase, dynamin (Dmn1), which is able to drive the final scission of the mitochondrion (5). No homologs for Mdv1 have been found in *Toxoplasma gondii*, but there are one Fis1 homolog (TGGT1_263323) and three dynamin-related proteins: DrpA, DrpB, and DrpC. Of these Drp proteins, DrpC, which lacks many of the features required for Drp function, has been associated with mitochondrial division (9). Nonetheless, we and other groups have shown that instead DrpC appears to be involved in vesicle trafficking and endocytosis (9, 10). As Fis1 is the strongest homolog of any putative fission protein in *Toxoplasma*, we investigated the role of Fis1 in monensin-driven mitochondrial rearrangement. We found that Fis1 localization to the mitochondrion is important for monensin-induced remodeling and that the absence of Fis1 results in decreased sensitivity to the ionophore. Thus, it is plausible that Fis1 is recruiting proteins to the mitochondrion outer membrane during monensin treatment to induce a transient constriction, similar to the transient interaction Fis1 has with Drp1 (27, 28). As DrpC and Fis1 do not seem to interact and DrpC localization does not change upon monensin treatment, it is unlikely that DrpC is involved in this process. Interactome analysis of Fis1 identified some proteins with domains of interest that are also found in Fis1 interactors of other systems. For example, TGGT1_224270 contains WD40-like domains, which is common to the Fis1 adaptor proteins (27, 29). TGGT1_304990 is a guanylate-binding protein that may be able to take the role of a dynamin-related protein in this system.

While Fis1 is essential in yeast, mammalian cells appear to have several proteins able to recruit the fission machinery, which makes Fis1 dispensable in those organisms. Knockout of *Toxoplasma* Fis1 does not disrupt mitochondrial morphology (30) or affect parasite fitness (21, 30). These results are corroborated by our experiments in which the

endogenous Fis1 gene was disrupted through CRISPR/Cas9 (see Fig. S1 in the supplemental material). Interestingly, we do observe a significant defect in the morphology of the mitochondrion when the endogenous Fis1 is mislocalized to the cytoplasm. In both mammalian cells and in yeast, either mislocalization or overexpression of Fis1 results in disruption of mitochondrial morphology (27, 31). In *Toxoplasma*, mislocalization of Fis1 resulted in aberrant mitochondrial morphology in which they maintain their lasso shape, but it is stretched out and appears to have strenuous branches and material. The phenotype observed with mislocalized Fis1 could be the consequence of Fis1 interacting with proteins that it would normally not come into contact with or of Fis1 pulling proteins away from the mitochondrial membrane where they are required. With this in mind, we performed a yeast two-hybrid screen to identify putative interactors. Interestingly, among the 24 proteins identified, seven (TGGT1_215520, TGGT1_218560, TGGT1_265180, TGGT1_246720, TGGT1_304990, TGGT1_321370, and TGGT1_321450) likely localize to the mitochondrion, based on a proteomic analysis of the *Toxoplasma* mitochondrion, which uses both *BirA (32) and ascorbate peroxidase (APEX) (33, 34) to identify novel mitochondrial proteins (35). Nonetheless, this proteome may not contain all the potential interactors that localize to the mitochondrion because the proteome was generated using a mitochondrial matrix protein, HSP70, thus excluding proteins that are localized to the outer mitochondrial membrane. *In silico* analysis of the putative Fis1 interactors using MitoProt, SignalP, and PSort (36–38) shows that an additional five proteins (TGGT1_226050, TGGT1_237015, TGGT1_247700, TGGT1_299670, and TGGT1_286470) may also localize to the mitochondrion based on the presence of mitochondrial signal. Another protein of interest is TGGT1_287980 has a forkhead-associated (FHA) domain, which is involved in a number of regulatory and signaling processes (39). Further characterization of these proteins is needed to determine what role they may play in mitochondrial remodeling and dynamics.

In this study, we focused on one of the putative Fis1 interactors, TGGT1_265180, which we have dubbed LMF1. This protein was the only protein identified through both the Y2H and a small-scale coimmunoprecipitation assay. LMF1 localizes to the OMM despite the absence of any domain or modification that would predict mitochondrial or membrane localization, suggesting that its association with the mitochondrion is likely through protein-protein interactions. When Fis1 is mislocalized to the cytoplasm, LMF1 expression is significantly reduced, and while some LMF1 is still deposited on the mitochondrion, other remnants do not appear to be associated with the organelle. LMF1 may not colocalize with Fis1 in these parasites because either protein may be interacting with other proteins or membranes. In the case of LMF1, there are potentially redundant interactors on the mitochondrial surface or interactors localized to other parts of the parasite, like the IMC, that are important for maintaining the mitochondrial lasso shape. Additionally, the expression level of LMF1 is decreased significantly when Fis1 is mislocalized, which may be due to either a decrease in the transcript level of LMF1 or due to the protein being degraded in the absence of potentially stabilizing Fis1 interactions.

Genetic disruption of LMF1 reveals its unexpected role in maintenance of mitochondrial morphology in intracellular parasites. LMF1 knockout results in loss of the typical lasso arrangement with the majority of parasites having either sperm-like or collapsed mitochondria. Thus, it appears that in the absence of LMF1, the mitochondrion of intracellular parasites adopts morphology normally only seen in extracellular ones. These mitochondrial morphologies, sperm-like and collapsed, are proposed to be due to a retraction of the mitochondrion from the IMC, as the parasite transitions to the extracellular environment. Therefore, it is possible that elimination of LMF1 has also eliminated these contact sites, causing a significant decrease in parasites with lasso morphology intracellularly. Membrane contact sites (MCSs) play important roles in signaling, lipid and ion exchange between organelles, and proper organelle positioning (40, 41). Whether any of these processes are affected in the LMF1 mutant strain is yet to be investigated. Nonetheless, the fact that parasites lacking LMF1 exhibit a propa-

gation defect suggest that the proper morphology of the mitochondrion is important for parasite fitness.

We noted that complementation of the knockout strain with the wild-type LMF1 was incomplete. While the exogenous copy was under the control of the *LMF1* promoter, it is possible that the expression level from the ectopic site is not at the right level for complete complementation. Another possibility is that, in order to adapt to the lack of LMF1, the expression of other factors required for mitochondrial morphology was affected. It is also plausible that that the addition of an epitope tag in the exogenous protein affects function or protein-protein interactions. Nonetheless, we have not observed any mitochondrial defect when epitope tags are added in the endogenous LMF1. Future experiments using conditional knockout of LMF1 will provide a better controlled system to study this mechanism.

Altering mitochondrial morphology is important in many systems to accommodate energetic needs and change positioning of organelles to perform specific functions. For example, *Trypanosoma brucei* is another parasite that contains a single mitochondrion that alters its shape in different life stages (42). During the procyclic phase in the tsetse fly midgut, the mitochondrion elongates to form an elaborate network of mitochondrial branches. In the bloodstream form, the branches collapse to form one tubule that lacks the respiratory capability of the procyclic stage. This mitochondrial morphology change is dependent on a protein called *T. brucei* LOK1 (TbLOK1), which is naturally downregulated in the bloodstream form (42). Based on this knowledge, it is possible that the retraction from the IMC toward the apical end of the parasite during extracellular stress is to (i) position the mitochondrion to the area of greatest energetic need and/or (ii) accommodate to the available nutrients. We propose that LMF1 interacts with Fis1 on the OMM and another or multiple proteins in the parasite pellicle to establish membrane contact sites to maintain the typical lasso shape. Upon egress, LMF1 or its interactors is either posttranslationally modified or downregulated so as to eliminate these contact sites and position the mitochondrion toward the apical end. Once the parasite has reentered a host cell, the mitochondrion can then reattach to the pellicle and can extend to the parasite periphery. LMF1 knockout parasites cannot properly form this lasso and therefore have given us an incredible tool to study the functional relevance of the mitochondrial morphodynamics and to identify the key players in this process.

MATERIALS AND METHODS

Host cell and parasite maintenance. All parasite strains were maintained via continued passage through human foreskin fibroblasts (HFFs) (purchased from ATCC) in normal growth medium, which consisted of Dulbecco's modified Eagle's medium (DMEM) supplemented with 10% fetal bovine serum (FBS), 2 mM L-glutamine, and 100 U penicillin/100 μg streptomycin per ml. All cultures were grown in a humidified incubator at 37°C and 5% CO_2. Parasites used were of the strain RH lacking hypoxanthine-xanthine-guanine phosphoribosyltransferase (HPT) (RHΔ*hpt*) (43) and RH lacking HPT and Ku80 (RHΔ*ku80*Δ*hpt*, referred to as Δ*ku80* thereafter) (44, 45). For experiments involving drug treatment, the medium was supplemented with 1% FBS rather than 10% FBS. For pyrimethamine treatment, we used dialyzed serum. All drugs were purchased from Sigma. Stocks of monensin, pyrimethamine, and myxothiazol were prepared in ethanol, while atovaquone was prepared in dimethyl sulfoxide (DMSO).

Generation of transgenic parasites. Parasites were engineered to express ectopic copies of full-length Fis1 (TGGT1_263323) or a truncated version lacking the putative transmembrane (TM) domain. For this purpose, PCR was utilized to amplify the Fis1 cDNA and append a hemagglutinin (HA) tag at the N terminus. The amplicon was flanked by NsiI and PacI restriction enzyme sites. Table S2 in the supplemental material lists all the primers used throughout this study. Purified PCR fragments were inserted into the pHEX2 plasmid (46) using the In-Fusion HD Cloning Plus kit (Clontech). Expression of the transgenes was controlled by the *SAG1* promoter, and selection was provided by the presence of the HPT selectable marker (43). KpnI-linearized plasmids (35 μg) were electroporated into parental RHΔ*hpt* parasites (47), and selection of parasites that successfully integrated the plasmid was achieved by growing parasites in medium containing 50 μg mycophenolic acid per ml and 50 μg xanthine per ml. Three rounds of drug selection were followed by limited dilution cloning to establish HA tag-positive parasite lines with and without the transmembrane domain termed RHΔ*hpt*+HAFis1 and RHΔ*hpt*+Fis1ΔTM, respectively.

To generate a parasite line expressing an endogenous Fis1 lacking the TM (RHΔ*ku80*:Fis1ΔTM), a fragment of the Fis1 gene comprising the region just upstream of the TM and flanked by PacI and AvrII was PCR amplified from *Toxoplasma* genomic DNA and inserted into the pLIC-HA(3x)-DHFR plasmid (44)

by In-Fusion cloning. EcoRV-linearized plasmid (35 μg) was transfected into Δ*ku80* parasites (44). The resulting transfectants were selected for dihydrofolate reductase (DHFR) by growth in medium with 1 μM pyrimethamine and cloned by limited dilution.

For C-terminal endogenous epitope tagging of TGGT1_265180, a PacI-flanked fragment of TGGT1_265180 just upstream of its stop codon was PCR amplified and inserted into pLIC-myc(3x)-DHFR by In-Fusion cloning. XcmI-linearized plasmid (60 μg) was transfected into Δ*ku80* parasites, and transfectants were selected for DHFR as described above.

Double homologous replacement of the TGGT1_265180 coding sequence was used to establish a knockout strain. For this purpose, we generated a knockout construct using the previously described pminiGFP vector (48). Using In-Fusion cloning, we introduced a 1,400-bp PCR amplicon encompassing the region upstream of the TGGT1_265180 start codon into the HindIII restriction site of pminiGFP and a 1,156-bp amplicon of the region downstream of the stop codon into the NotI restriction site. In this manner, the resulting vector (p265180_KO [KO stands for knockout]) has a drug selection cassette, HPT, flanked by regions of homology to the sequences upstream and downstream of TGGT1_265180. Ten micrograms of DraIII-linearized p265180_KO was transfected into Δ*ku80* parasites using Nucleofector (Lonza), and parasites were then selected for the expression of HPT as described above. Disruption of TGGT1_265180 was confirmed by PCR using three primer sets (Table S2). The first primer set (P1) amplifies a 637-bp region present in wild-type parasites and absent in the knockout strain (Fig. 7A). The second primer set (P2) was designed to amplify a 1,933-bp fragment present only if the double homologous recombination of the knockout construct occurred at the TGGT1_265180 locus (Fig. 7A). The final primer set (P3) amplifies a fragment in both the wild-type and knockout strains (Fig. 7A).

For exogenous expression of TGGT1_265180, a 3,700-bp fragment beginning approximately 2 kb upstream of the TGGT1_265180 start codon and ending at its stop codon was PCR amplified from genomic DNA. This PCR amplicon was inserted into the PacI site of pLIC-HA(3x)-DHFR by In-Fusion cloning. The same method was used to create a plasmid lacking the predicted selected interaction domain (SID), thus truncating the gene. These plasmids were used as the templates to amplify an 8-kb fragment that included the TGGT1_265180 gene under the control of its own promoter, a triple hemagglutinin tag, and the DHFR drug selection cassette. Primers used included overhangs homologous to the remnants of the Δ*ku80* site on each side of a double-stranded cut created by CRISPR/Cas9. The 8-kb PCR fragment was gel extracted using the NucleoSpin Gel and PCR Clean-up kit (Macherey-Nagel) and eluted in P3 buffer (Lonza) for nucleofection. The pSAG1-Cas9-U6-sgUPRT plasmid, generously provided by the Sibley lab (18), was mutated to contain a guide RNA targeted to the Ku80 site. TGGT1_265180 knockout and parental parasites were transfected with 1 μg of either the full-length (265180-HA) or truncated (265180ΔSID-HA) PCR amplicons and 2 μg of pSAG1-Cas9-sgKu80 using the Nucleofector (Lonza). Parasites were selected for the presence of DHFR as described above. Immunofluorescence and Western blotting (see below) were used to confirm expression and localization of the exogenous copies of TGGT1_265180.

Immunofluorescence microscopy analysis. For immunofluorescence assay (IFA), infected HFFs were fixed with 3.5% formaldehyde, quenched with 100 mM glycine, and blocked and permeabilized in phosphate-buffered saline (PBS) containing 3% bovine serum albumin (BSA) and 0.2% Triton X-100 (TX-100) (PBS/3% BSA/0.2% TX-100). Samples were then incubated with primary antibodies in PBS/3% BSA/0.2% TX-100 for 1 h, washed five times with PBS, and incubated with Alexa Fluor-conjugated secondary antibodies in PBS/3% BSA for 1 h. The coverslips were washed with PBS and mounted on glass slides with 3 μl 4′,6′-diamidino-2-phenylindole (DAPI) containing Vectashield. For three-dimensional structured illumination microscopy (3D-SIM), coverslips were stained with a liquid DAPI solution in PBS, washed, and inverted on a glass slide with Vectashield mounting medium without DAPI. Image acquisition and processing were performed on either a Nikon Eclipse 80i microscope with NIS-Elements AR 3.0 software or a Leica DMI6000 B microscope with LAS X 1.5.1.13187 software. 3D-SIM was performed utilizing the OMX 3D-SIM superresolution system located within the Light Microscopy Imaging Center at Indiana University Bloomington (https://biochemistry.indiana.edu/labs-facilities/iu-facilities/light-microscopy.html). The system is equipped with four Photometrics Cascade II electron-multiplying charge-coupled-device (EMCCD) cameras that permit imaging four colors simultaneously and is controlled by DV-OMX software. Image processing was completed using the Applied Precision softWoRx software.

Primary antibodies used in this study included rabbit anti-HA (Cell Signaling Technology), rabbit anti-myc (Cell Signaling Technology), a rabbit polyclonal antibody against the MORN1 protein (49), mouse monoclonal antibody 5F4 (detects F_1B ATPase; P. Bradley, unpublished results), and rabbit anti-acetyl-K40-α-tubulin (catalog no. ABT241; EMD Millipore), all used at 1:1,000, with the exception of 5F4 which was used at 1:5,000. Secondary antibodies included Alexa Fluor 594- or Alexa Fluor 488-conjugated goat anti-rabbit and goat anti-mouse (Invitrogen), all used at 1:2,000.

Phenotypic characterization of mutant and complemented strains. For drug effects on mitochondrial morphology, infected HFFs on coverslips were vehicle or drug treated with monensin (1 ng/ml), atovaquone (100 nM), pyrimethamine (1 μM), or myxothiazol (50 ng/ml) for 12 h. To allow for recovery, drug-containing medium was washed away and replaced with normal growth medium for an additional 12 h. IFA was performed as described above using F_1B ATPase antibodies to monitor the mitochondrion. Samples were examined in a blind manner, and at least 100 vacuoles per sample were inspected. Experiments were performed in experimental and biological triplicates.

Plaque and doubling assays were performed with 12-well plates using standard methods (50). Briefly, for the plaque assays, 500 freshly egressed parasites were added to confluent HFF monolayers. After 4 days of incubation, cultures were fixed with methanol for 5 min and stained with crystal violet. Plaques

were imaged using a ProteinSimple imaging system, and the number of plaques was counted by using a light microscope. Experiments were performed in experimental and biological triplicates.

Yeast two-hybrid screen. Yeast two-hybrid (Y2H) screening was performed by Hybrigenics Services, S.A.S., Paris, France. The coding sequence for Fis1 (amino acids [aa] 2 to 118; GenBank accession no. XM_018781322.1) was PCR amplified and cloned into pB66 as a C-terminal fusion with the Gal4 DNA-binding domain (Gal4-Fis1). The construct was checked by sequencing and used as a bait to screen a random-primed *Toxoplasma* cDNA library constructed in pP6. pB66 derives from the original pAS2ΔΔ vector (51), and pP6 is based on the pGADGH plasmid (52). Forty-six million clones (5-fold the complexity of the library) were screened using a mating approach with YHGX13 (Y187 *ade2-101*::*loxP-kanMX-loxP mat*α) and CG1945 (*mat*α) yeast strains as previously described (51). A total of 247 His-positive (His+) colonies were selected on a medium lacking tryptophan, leucine, and histidine. The prey fragments of the positive clones were amplified by PCR and sequenced at their 5′ and 3′ junctions. The resulting sequences were used to identify the corresponding interacting proteins in the GenBank database (NCBI) using a fully automated procedure. A confidence score (predicted biological score [PrBS]) was attributed to each interaction as previously described (53).

Immunoprecipitation assay. To confirm the results of the yeast two-hybrid screening, we performed one immunoprecipitation assay using RHΔ*hpt*+HAFis1, with the parental RHΔ*hpt* parasites as a negative control. Extracellular parasites from 10 T175 culture flasks were spun down, washed twice with cold PBS, and resuspended in Pierce coimmunoprecipitation (Co-IP) lysis buffer (Thermo Fisher Scientific) with protease/phosphatase inhibitor cocktail (100×, Cell Signaling Technology). After 1 h of lysis at 4°C, the samples were sonicated three times for 15 s each time, with 1-min rest period between each sonication. After sonication, samples were pelleted, and the supernatant was transferred to Pierce anti-HA magnetic beads (Thermo Fisher Scientific). Samples were placed on a rocker at 4°C for 2.5 h before beads were washed once with Pierce Co-IP lysis buffer and twice with PBS. Beads were resuspended in 8 M urea and sent for liquid chromatography coupled to tandem mass spectrometry (LC/MS-MS) analysis. Results were narrowed down to proteins that had at least four peptides in the RHΔ*hpt*+HAFis1 sample and none in the RHΔ*hpt* control. This shortened list was then compared to the list of putative interactors obtained through yeast two-hybrid assay.

Western blots. Extracellular parasites were pelleted and resuspended in 2× Laemmli sample buffer (Bio-Rad) with 5% 2-mercaptoethanol (Sigma-Aldrich). Samples were boiled for 5 min at 95°C before separation on a gradient 4 to 20% sodium dodecyl sulfate (SDS)-polyacrylamide gel (Bio-Rad). Samples were then transferred to nitrocellulose membrane using standard methods for semidry transfer (Bio-Rad). Membranes were probed with rabbit anti-HA (Cell Signaling Technologies), mouse anti-c-*myc* (Cell Signaling Technologies), or mouse anti-SAG1 (Thermo Fisher Scientific) at a dilution of 1:5,000 for 1 h. Membranes were then washed and probed with either goat anti-mouse horseradish peroxidase or goat anti-rabbit horseradish peroxidase (Sigma-Aldrich) at a dilution of 1:10,000 for 1 h (GE Healthcare). Proteins were detected using SuperSignal West Femto substrate (Thermo Fisher) and imaged using the FluorChem R system (Biotechne). All original Western blots are shown in Data Set S2 in the supplemental material.

For comparative analysis of LMF1 protein levels in RHΔ*ku80*:Fis1ΔTM parasites to the levels in RHΔ*ku80* parasites, the parasites were centrifuged and washed once with PBS. Parasites were counted using a hemocytometer, and the parasite pellets were resuspended at appropriate volumes to equilibrate the concentration of parasites. The subsequent immunoblots were then probed for anti-SAG1 as a loading control. ImageJ was used for densitometry analysis of the detected protein band and compared to SAG1 signal. The ratio of LMF1 protein levels (normalized to the SAG1 levels in the same sample) of RHΔ*ku80*:Fis1ΔTM to RHΔ*ku80* parasites was determined and represented as a percentage. These determinations were done in biological triplicate, and the described percentage is an average of these replicates.

Statistical analysis. Statistics were performed with either JMP14.0 or Prism software.

SUPPLEMENTAL MATERIAL

Supplemental material is available online only.

FIG S1, PDF file, 1 MB.

FIG S2, PDF file, 0.8 MB.

FIG S3, PDF file, 0.9 MB.

TABLE S1, PDF file, 0.03 MB.

TABLE S2, PDF file, 0.03 MB.

DATA SET S1, XLSX file, 0.02 MB.

DATA SET S2, PDF file, 1.3 MB.

ACKNOWLEDGMENTS

This work was funded by grants from the National Institutes of Health to G.A. (R01AI123457 and R21AI138255). K.J. is funded by a fellowship from NRSA training grant T32AI060519. R.C. was funded by a fellowship from the American Heart Association (15POST22740002).

The funders had no role in study design, data collection and interpretation, or the decision to submit the work for publication.

We thank Hybrigenics for their analyses and support using Y2H. We also thank Peter Bradley for generously providing F_1B ATPase antibody.

REFERENCES

1. Webster JP. 2010. Dubey, J.P Toxoplasmosis of animals and humans. Parasit Vectors 3:112. https://doi.org/10.1186/1756-3305-3-112.
2. Melo EJL, Attias M, De Souza W. 2000. The single mitochondrion of tachyzoites of *Toxoplasma gondii*. J Struct Biol 130:27–33. https://doi.org/10.1006/jsbi.2000.4228.
3. Kovacs JA. 1992. Efficacy of atovaquone in treatment of toxoplasmosis in patients with AIDS. The NIAID-Clinical Center Intramural AIDS Program. Lancet 340:637–638. https://doi.org/10.1016/0140-6736(92)92172-c.
4. Nishi M, Hu K, Murray JM, Roos DS. 2008. Organellar dynamics during the cell cycle of *Toxoplasma gondii*. J Cell Sci 121:1559–1568. https://doi.org/10.1242/jcs.021089.
5. van der Bliek AM. 2000. A mitochondrial division apparatus takes shape. J Cell Biol 151:f1–f4. https://doi.org/10.1083/jcb.151.2.f1.
6. Osellame LD, Singh AP, Stroud DA, Palmer CS, Stojanovski D, Ramachandran R, Ryan MT. 2016. Cooperative and independent roles of the Drp1 adaptors Mff, MiD49 and MiD51 in mitochondrial fission. J Cell Sci 129:2170–2181. https://doi.org/10.1242/jcs.185165.
7. Breinich MS, Ferguson DJP, Foth BJ, van Dooren GG, Lebrun M, Quon DV, Striepen B, Bradley PJ, Frischknecht F, Carruthers VB, Meissner M. 2009. A dynamin is required for the biogenesis of secretory organelles in *Toxoplasma gondii*. Curr Biol 19:277–286. https://doi.org/10.1016/j.cub.2009.01.039.
8. van Dooren GG, Reiff SB, Tomova C, Meissner M, Humbel BM, Striepen B. 2009. A novel dynamin-related protein has been recruited for apicoplast fission in *Toxoplasma gondii*. Curr Biol 19:267–276. https://doi.org/10.1016/j.cub.2008.12.048.
9. Heredero-Bermejo I, Varberg JM, Charvat R, Jacobs K, Garbuz T, Sullivan WJ, Arrizabalaga G. 2019. TgDrpC, an atypical dynamin-related protein in *Toxoplasma gondii*, is associated with vesicular transport factors and parasite division. Mol Microbiol 111:46–64. https://doi.org/10.1111/mmi.14138.
10. Amiar S, Katris NJ, Berry L, Dass S, Shears MJ, Brunet C, Touquet B, Hakimi M-A, McFadden GI, Yamaryo-Botté Y, Botté CY. 2019. Division and adaptation to host nutritional environment of apicomplexan parasites depend on apicoplast lipid metabolic plasticity and host organelles remodelling. bioRxiv https://doi.org/10.1101/585737.
11. Ovciarikova J, Lemgruber L, Stilger KL, Sullivan WJ, Sheiner L. 2017. Mitochondrial behaviour throughout the lytic cycle of *Toxoplasma gondii*. Sci Rep 7:42746. https://doi.org/10.1038/srep42746.
12. Prinz WA. 2014. Bridging the gap: membrane contact sites in signaling, metabolism, and organelle dynamics. J Cell Biol 205:759–769. https://doi.org/10.1083/jcb.201401126.
13. Charvat RA, Arrizabalaga G. 2016. Oxidative stress generated during monensin treatment contributes to altered *Toxoplasma gondii* mitochondrial function. Sci Rep 6:22997. https://doi.org/10.1038/srep22997.
14. Lavine MD, Arrizabalaga G. 2012. Analysis of monensin sensitivity in *Toxoplasma gondii* reveals autophagy as a mechanism for drug induced death. PLoS One 7:e42107. https://doi.org/10.1371/journal.pone.0042107.
15. Thierbach G, Reichenbach H. 1981. Myxothiazol, a new inhibitor of the cytochrome b-c1 segment of the respiratory chain. Biochim Biophys Acta 638:282–289. https://doi.org/10.1016/0005-2728(81)90238-3.
16. Garbuz T, Arrizabalaga G. 2017. Lack of mitochondrial MutS homolog 1 in *Toxoplasma gondii* disrupts maintenance and fidelity of mitochondrial DNA and reveals metabolic plasticity. PLoS One 12:e0188040. https://doi.org/10.1371/journal.pone.0188040.
17. Padgett LR, Arrizabalaga G, Sullivan WJ. 2017. Targeting of tail-anchored membrane proteins to subcellular organelles in *Toxoplasma gondii*. Traffic 18:149–158. https://doi.org/10.1111/tra.12464.
18. Shen B, Brown KM, Lee TD, Sibley LD. 2014. Efficient gene disruption in diverse strains of *Toxoplasma gondii* using CRISPR/CAS9. mBio 5:e01114-14. https://doi.org/10.1128/mBio.01114-14.
19. Rain JC, Selig L, De Reuse H, Battaglia V, Reverdy C, Simon S, Lenzen G, Petel F, Wojcik J, Schächter V, Chemama Y, Labigne A, Legrain P. 2001. The protein-protein interaction map of Helicobacter pylori. Nature 409:211–215. https://doi.org/10.1038/35051615.
20. Wojcik J, Boneca IG, Legrain P. 2002. Prediction, assessment and validation of protein interaction maps in bacteria. J Mol Biol 323:763–770. https://doi.org/10.1016/s0022-2836(02)01009-4.
21. Sidik SM, Huet D, Ganesan SM, Huynh M-H, Wang T, Nasamu AS, Thiru P, Saeij JPJ, Carruthers VB, Niles JC, Lourido S. 2016. A genome-wide CRISPR screen in *Toxoplasma* identifies essential apicomplexan genes. Cell 166:1423–1435.e12. https://doi.org/10.1016/j.cell.2016.08.019.
22. Hu K, Mann T, Striepen B, Beckers CJM, Roos DS, Murray JM. 2002. Daughter cell assembly in the protozoan parasite *Toxoplasma gondii*. Mol Biol Cell 13:593–606. https://doi.org/10.1091/mbc.01-06-0309.
23. Tondera D, Grandemange S, Jourdain A, Karbowski M, Mattenberger Y, Herzig S, Da Cruz S, Clerc P, Raschke I, Merkwirth C, Ehses S, Krause F, Chan DC, Alexander C, Bauer C, Youle R, Langer T, Martinou J-C. 2009. SLP-2 is required for stress-induced mitochondrial hyperfusion. EMBO J 28:1589–1600. https://doi.org/10.1038/emboj.2009.89.
24. Visser W, van Spronsen EA, Nanninga N, Pronk JT, Kuenen JG, van Dijken JP. 1995. Effects of growth conditions on mitochondrial morphology in Saccharomyces cerevisiae. Antonie Van Leeuwenhoek 67:243–253. https://doi.org/10.1007/bf00873688.
25. De Vos KJ, Allan VJ, Grierson AJ, Sheetz MP. 2005. Mitochondrial function and actin regulate dynamin-related protein 1-dependent mitochondrial fission. Curr Biol 15:678–683. https://doi.org/10.1016/j.cub.2005.02.064.
26. Mendl N, Occhipinti A, Müller M, Wild P, Dikic I, Reichert AS. 2011. Mitophagy in yeast is independent of mitochondrial fission and requires the stress response gene WHI2. J Cell Sci 124:1339–1350. https://doi.org/10.1242/jcs.076406.
27. Stojanovski D, Koutsopoulos OS, Okamoto K, Ryan MT. 2004. Levels of human Fis1 at the mitochondrial outer membrane regulate mitochondrial morphology. J Cell Sci 117:1201–1210. https://doi.org/10.1242/jcs.01058.
28. Yu R, Jin S, Lendahl U, Nistér M, Zhao J. 2019. Human Fis1 regulates mitochondrial dynamics through inhibition of the fusion machinery. EMBO J 38:e99748. https://doi.org/10.15252/embj.201899748.
29. Zhang Y, Chan DC. 2007. Structural basis for recruitment of mitochondrial fission complexes by Fis1. Proc Natl Acad Sci U S A 104:18526–18530. https://doi.org/10.1073/pnas.0706441104.
30. Melatti C, Pieperhoff M, Lemgruber L, Pohl E, Sheiner L, Meissner M. 2019. A unique dynamin-related protein is essential for mitochondrial fission in *Toxoplasma gondii*. PLoS Pathog 15:e1007512. https://doi.org/10.1371/journal.ppat.1007512.
31. James DI, Parone PA, Mattenberger Y, Martinou J-C. 2003. hFis1, a novel component of the mammalian mitochondrial fission machinery. J Biol Chem 278:36373–36379. https://doi.org/10.1074/jbc.M303758200.
32. Roux KJ, Kim DI, Raida M, Burke B. 2012. A promiscuous biotin ligase fusion protein identifies proximal and interacting proteins in mammalian cells. J Cell Biol 196:801–810. https://doi.org/10.1083/jcb.201112098.
33. Rhee H-W, Zou P, Udeshi ND, Martell JD, Mootha VK, Carr SA, Ting AY. 2013. Proteomic mapping of mitochondria in living cells via spatially restricted enzymatic tagging. Science 339:1328–1331. https://doi.org/10.1126/science.1230593.
34. Hung V, Zou P, Rhee H-W, Udeshi ND, Cracan V, Svinkina T, Carr SA, Mootha VK, Ting AY. 2014. Proteomic mapping of the human mitochondrial intermembrane space in live cells via ratiometric APEX tagging. Mol Cell 55:332–341. https://doi.org/10.1016/j.molcel.2014.06.003.
35. Seidi A, Muellner-Wong LS, Rajendran E, Tjhin ET, Dagley LF, Aw VY, Faou P, Webb AI, Tonkin CJ, van Dooren GG. 2018. Elucidating the mitochondrial proteome of *Toxoplasma gondii* reveals the presence of a divergent cytochrome c oxidase. Elife 7:e38131. https://doi.org/10.7554/eLife.38131.
36. Nakai K, Horton P. 1999. PSORT: a program for detecting sorting signals in proteins and predicting their subcellular localization. Trends Biochem Sci 24:34–36. https://doi.org/10.1016/s0968-0004(98)01336-x.
37. Claros MG, Vincens P. 1996. Computational method to predict mitochondrially imported proteins and their targeting sequences. Eur J Biochem 241:779–786. https://doi.org/10.1111/j.1432-1033.1996.00779.x.
38. Armenteros JJA, Tsirigos KD, Sønderby CK, Petersen TN, Winther O, Brunak S, von Heijne G, Nielsen H. 2019. SignalP 5.0 improves signal peptide predictions using deep neural networks. Nat Biotechnol 37:420–423. https://doi.org/10.1038/s41587-019-0036-z.

39. Durocher D, Jackson SP. 2002. The FHA domain. FEBS Lett 513:58–66. https://doi.org/10.1016/s0014-5793(01)03294-x.
40. Helle SCJ, Kanfer G, Kolar K, Lang A, Michel AH, Kornmann B. 2013. Organization and function of membrane contact sites. Biochim Biophys Acta 1833:2526–2541. https://doi.org/10.1016/j.bbamcr.2013.01.028.
41. Eisenberg-Bord M, Shai N, Schuldiner M, Bohnert M. 2016. A tether is a tether is a tether: tethering at membrane contact sites. Dev Cell 39:395–409. https://doi.org/10.1016/j.devcel.2016.10.022.
42. Povelones ML, Tiengwe C, Gluenz E, Gull K, Englund PT, Jensen RE. 2013. Mitochondrial shape and function in trypanosomes requires the outer membrane protein, TbLOK1. Mol Microbiol 87:713–729. https://doi.org/10.1111/mmi.12089.
43. Donald RGK, Carter D, Ullman B, Roos DS. 1996. Insertional tagging, cloning, and expression of the *Toxoplasma gondii* hypoxanthine-xanthine-guanine phosphoribosyltransferase gene: use as a selectable marker. J Biol Chem 271:14010–14019. https://doi.org/10.1074/jbc.271.24.14010.
44. Huynh M, Carruthers V. 2009. Tagging of endogenous genes in a *Toxoplasma gondii* strain lacking Ku80. Eukaryot Cell 8:530–539. https://doi.org/10.1128/EC.00358-08.
45. Fox B, Ristuccia J, Gigley J, Bzik D. 2009. Efficient gene replacements in *Toxoplasma gondii* strains deficient for nonhomologous end joining. Eukaryot Cell 8:520–529. https://doi.org/10.1128/EC.00357-08.
46. Saeij JPJ, Arrizabalaga G, Boothroyd JC. 2008. A cluster of four surface antigen genes specifically expressed in bradyzoites, SAG2CDXY, plays an important role in *Toxoplasma gondii* persistence. Infect Immun 76:2402–2410. https://doi.org/10.1128/IAI.01494-07.
47. Donald R, Roos D. 1998. Gene knock-outs and allelic replacements in *Toxoplasma gondii*: HXGPRT as a selectable marker for hit-and-run mutagenesis. Mol Biochem Parasitol 91:295–305. https://doi.org/10.1016/s0166-6851(97)00210-7.
48. Arrizabalaga G, Ruiz F, Moreno S, Boothroyd JC. 2004. Ionophore-resistant mutant of *Toxoplasma gondii* reveals involvement of a sodium/hydrogen exchanger in calcium regulation. J Cell Biol 165:653–662. https://doi.org/10.1083/jcb.200309097.
49. Gubbels M-J, Vaishnava S, Boot N, Dubremetz J-F, Striepen B. 2006. A MORN-repeat protein is a dynamic component of the *Toxoplasma gondii* cell division apparatus. J Cell Sci 119:2236–2245. https://doi.org/10.1242/jcs.02949.
50. LaFavers KA, Márquez-Nogueras KM, Coppens I, Moreno SNJ, Arrizabalaga G. 2017. A novel dense granule protein, GRA41, regulates timing of egress and calcium sensitivity in *Toxoplasma gondii*. Cell Microbiol 19:e12749. https://doi.org/10.1111/cmi.12749.
51. Fromont-Racine M, Rain J-C, Legrain P. 1997. Toward a functional analysis of the yeast genome through exhaustive two-hybrid screens. Nat Genet 16:277–282. https://doi.org/10.1038/ng0797-277.
52. Bartel PL, Chien CT, Sternglanz R, Fields S. 1993. Using the two-hybrid system to detect protein-protein interactions, p 153–179. *In* Hartley DA (ed), Cellular interactions in development: a practical approach. Oxford University Press, Oxford, United Kingdom.
53. Formstecher E, Aresta S, Collura V, Hamburger A, Meil A, Trehin A, Reverdy C, Betin V, Maire S, Brun C, Jacq B, Arpin M, Bellaiche Y, Bellusci S, Benaroch P, Bornens M, Chanet R, Chavrier P, Delattre O, Doye V, Fehon R, Faye G, Galli T, Girault J-A, Goud B, de Gunzburg J, Johannes L, Junier M-P, Mirouse V, Mukherjee A, Papadopoulo D, Perez F, Plessis A, Rossé C, Saule S, Stoppa-Lyonnet D, Vincent A, White M, Legrain P, Wojcik J, Camonis J, Daviet L. 2005. Protein interaction mapping: a Drosophila case study. Genome Res 15:376–384. https://doi.org/10.1101/gr.2659105.